

**Band structures, lifetimes, and shape coexistence in  $^{130}\text{La}$** 

M. Ionescu-Bujor<sup>1</sup>, S. Aydin<sup>2</sup>, A. Iordăchescu<sup>1</sup>, N. Mărginean<sup>1</sup>, S. Pascu<sup>1</sup>, D. Bucurescu<sup>1</sup>, C. Costache<sup>1</sup>, N. Florea<sup>1</sup>, T. Glodariu<sup>1,\*</sup>, A. Ionescu<sup>1,3</sup>, R. Mărginean<sup>1</sup>, C. Mihai<sup>1</sup>, R. E. Mihai<sup>1</sup>, A. Mitu<sup>1</sup>, A. Negret<sup>1</sup>, C. R. Niță<sup>1</sup>, A. Olăcel<sup>1</sup>, B. Saygı<sup>4,5</sup>, L. Stroe<sup>1</sup>, R. Suvăilă<sup>1</sup>, S. Toma<sup>1</sup>, and A. Turturică<sup>1</sup>

<sup>1</sup>Horia Hulubei National Institute of Physics and Nuclear Engineering, 077125 Bucharest-Măgurele, Romania

<sup>2</sup>Department of Natural and Mathematical Sciences, Engineer Faculty, Tarsus University, 33400, Tarsus, Turkey

<sup>3</sup>Faculty of Physics, University of Bucharest, 077125 Bucharest-Măgurele, Romania

<sup>4</sup>Department of Physics, Faculty of Science, Ege University, Bornova, 35100 Izmir, Turkey

<sup>5</sup>Department of Physics, Faculty of Science and Arts, Sakarya University, 54187, Sakarya, Turkey



(Received 6 April 2020; revised 4 September 2020; accepted 24 September 2020; published 12 October 2020)

The level structure of  $^{130}\text{La}$  has been investigated using the  $^{121}\text{Sb}(^{12}\text{C}, 3n)$  reaction with the ROSPHERE array at IFIN-HH, Bucharest. The level scheme was significantly extended with the observation of 45 new states and 100 new transitions. Several band structures have been identified and a clear connection with the lower-lying states has been established. A lifetime of  $\tau = 3.6(2)$  ns has been measured for the 346-keV  $6^-$  state by the in-beam fast timing technique. The lifetimes of 18 high-spin states have been determined by applying the Doppler-shift attenuation method. The deformations derived from the experimental  $B(E2)$  transition strengths indicate distinct coexisting shapes at high spins in  $^{130}\text{La}$ . The experimental properties of both low- and high-spin states were compared with theoretical calculations performed in the frame of the two-quasiparticles-plus-rotor model. Two new negative-parity decoupled bands, with a deduced quadrupole deformation  $\beta_2 = 0.150(15)$ , were interpreted by coupling the proton in the  $1/2[550]$  and  $3/2[541]$  orbitals with the odd neutron occupying mainly the low- $\Omega$  orbitals from the  $d_{3/2}$  and  $s_{1/2}$  states. A quadrupole deformation  $\beta_2 = 0.220(17)$  was derived for a newly identified positive-parity decoupled band. This enhanced deformation was attributed to the involvement in the band configuration of the  $\Omega = 1/2$  ( $f_{7/2}, h_{9/2}$ ) intruder neutron orbital. The multiparticle configuration  $\pi g_{7/2}(h_{11/2})^2 \otimes \nu(h_{11/2})$  was assigned to a high-spin negative-parity dipole band, based on the comparison of the experimental  $B(M1)$  transition strengths with values calculated by applying the geometrical model of Dönau and Frauendorf.

DOI: [10.1103/PhysRevC.102.044311](https://doi.org/10.1103/PhysRevC.102.044311)

**I. INTRODUCTION**

The nuclei with mass number around 130 ( $55 \leq Z \leq 63$ ,  $68 \leq N \leq 78$ ), situated in the transitional zone between the nearly spherical region and the deformed region, are considered to be soft with respect to both the quadrupole deformation ( $\beta_2$ ) and the shape asymmetry ( $\gamma$ ). Detailed spectroscopic studies have revealed a variety of coexisting structures associated with specific orbitals. Particular interest has been devoted in the last two decades to the investigation on nuclear chirality as a direct evidence for triaxiality [1]. The different deformation-driving properties of neutrons and protons occupying the unique-parity subshell  $h_{11/2}$  in the high- $\Omega$  and low- $\Omega$  orbitals, respectively, may lead to the occurrence of triaxial shapes. The chirality manifests itself by the presence of two, almost degenerate  $\Delta J = 1$  rotational bands having the same parity and linked to each other by interband  $\gamma$ -ray transitions. Around 25 chiral nuclei have been identified in the  $A \approx 130$  region, the largest ensemble of nuclei exhibiting chiral bands in the table of elements [2]. Chiral partners with the configuration  $\pi h_{11/2} \otimes \nu h_{11/2}^{-1}$  have been observed in odd-odd

Cs, La, Pr, Pm, and Eu nuclei. Recently three-quasiparticle chiral bands have been observed in odd-mass  $^{133}\text{Ce}$  [3],  $^{133}\text{La}$  [4], and  $^{135}\text{Nd}$  [5,6], while four- and six-quasiparticle chiral bands were observed in the even-even  $^{136}\text{Nd}$  [7] and  $^{138}\text{Nd}$  [8] nuclei. In most nuclei only one chiral doublet was observed, however, in  $^{133}\text{Ce}$  [3],  $^{135}\text{Nd}$  [6], and  $^{136}\text{Nd}$  [7] two or more chiral doublets were identified, illustrating the exotic phenomenon of multiple chiral doublet bands.

Electromagnetic transition probabilities derived from lifetime measurements in the chiral bands are considered to provide crucial fingerprints for the chirality phenomenon. As specified in several theoretical calculations [9–11], the reduced transition strengths for the in-band transitions should be similar for both the bands. Moreover for the bands described by the  $\pi h_{11/2} \otimes \nu h_{11/2}^{-1}$  configuration the reduced transition probability ratios  $B(M1)/B(E2)$ , as well as the  $B(M1)$  values should exhibit odd-even staggering. Recent lifetime measurements in the chiral-partner bands of the odd-odd  $^{124-130}\text{Cs}$  nuclei [12–16] gave support to the chiral interpretation. On the other hand the reduced transition probabilities derived in  $^{132}\text{La}$  [14] and  $^{134}\text{Pr}$  [17] were found to be in disagreement with the chiral scenario.

Another important feature of nuclei in the  $A \approx 130$  mass region is the occurrence of rotational bands with highly

\*Deceased.

deformed prolate shapes ( $\beta_2 \approx 0.3\text{--}0.4$ ) that are coexisting with the normally deformed bands ( $\beta_2 \approx 0.2$ ) [18]. Around 45 rotational sequences having characteristics consistent with highly deformed prolate shapes have been observed in even-even, odd-mass, and odd-odd nuclei from La to Eu [18]. Detailed studies have revealed that the existence of highly deformed bands is the result of an interplay between microscopic shell effects, such as the occurrence of large gaps in nucleon single-particle energies and the involvement of specific orbitals. In this mass region they were interpreted as involving one or more neutrons in the  $1/2[660]$  ( $i_{13/2}$ ) Nilsson intruder orbital [19]. Despite intense experimental effort, in most cases it was not possible to link the highly deformed bands to the low-spin, normally deformed structures [18,20]. In a few Pr, Nd, Pm isotopes with  $N \leq 75$  low-lying bands involving the  $\nu(f_{7/2} + h_{9/2})$  configuration have been also observed [21–25]. Lifetime measurements revealed that this intruder neutron orbital leads to quadrupole deformation values, which are intermediate between those known for normally deformed and the highly deformed bands [23,26–28].

The aim of the present work is to enrich the knowledge of the odd-odd nucleus  $^{130}\text{La}$  ( $Z = 57, N = 73$ ) through detailed spectroscopic and lifetime measurements. The high-spin levels of this nucleus have been investigated in several previous experiments [29–33].  $^{130}\text{La}$  is one of the first nuclei in which a chiral doublet has been reported [33]. A highly deformed band with  $\beta_2 \approx 0.4$ , not linked to the lower-lying states, has been also observed [32]. Note that  $^{130}\text{La}$  is the only La isotope in which a highly deformed band has been reported [18].

In this paper we present experimental results that extend significantly the level scheme of  $^{130}\text{La}$  of both low and high spins. Lifetimes of high-spin states in several bands were derived by applying the Doppler-shift attenuation method (DSAM), while the in-beam fast timing method was used to determine lifetimes of lower-lying states. The results concerning the lifetimes in the chiral-partner bands were reported in Ref. [34]. The experimental details are briefly presented in Sec. II. The results including the level scheme and the lifetime measurements are presented in Sec. III, while in Sec. IV the properties of the level scheme are discussed.

## II. EXPERIMENTAL DETAILS AND DATA ANALYSIS

High-spin states in  $^{130}\text{La}$  were populated in the  $^{121}\text{Sb}(^{12}\text{C}, 3n)$  reaction at a beam energy of 54 MeV. The  $^{12}\text{C}$  beam was supplied by the FN Tandem accelerator of the Horia Hulubei National Institute of Physics and Nuclear Engineering (IFIN-HH) in Bucharest. A  $1\text{ mg/cm}^2$  isotopically enriched  $^{121}\text{Sb}$  layer evaporated on a  $50\text{ mg/cm}^2$   $^{208}\text{Pb}$  foil was used as target. The experimental setup consisted of the ROSPHERE mixed array [35], comprising 14 high-purity germanium detectors (HPGe) and 11  $\text{LaBr}_3(\text{Ce})$  scintillator detectors. The HPGe detectors were placed in three rings at the angles of  $143^\circ$ ,  $90^\circ$ , and  $37^\circ$  with respect to the beam axis. The  $\text{LaBr}_3(\text{Ce})$  scintillators were placed in angular rings at  $110^\circ$ ,  $90^\circ$ , and  $70^\circ$  with respect to the beam direction. Energy and efficiency calibrations were performed using a  $^{152}\text{Eu}$  source. In order to analyze the  $\gamma$ -ray coincidence relations and to construct the level scheme of  $^{130}\text{La}$  the collected events from

the HPGe detectors were sorted into a symmetric  $\gamma$ - $\gamma$ - $\gamma$  cube from which doubly gated spectra were extracted. The coincidence relations were also analyzed using a symmetric  $\gamma$ - $\gamma$  matrix. An energy-time matrix was created in order to investigate the time behavior for selected transitions. Information about the  $\gamma$  transition multipolarities was obtained from asymmetric matrices having the detectors in each ring on the first axis, and all detectors on the second axis. The  $\gamma$  intensities corrected for efficiencies, from spectra gated on the axis with all the detectors, were used to calculate the ratio  $R_{ADO}$  defined as [36]:  $R_{ADO} = [I_\gamma(37^\circ) + I_\gamma(143^\circ)]/2I_\gamma(90^\circ)$ . In the present experimental conditions typical  $R_{ADO}$  values are  $\approx 0.8$  for pure dipole stretched transitions, and  $\approx 1.4$  for quadrupole stretched transitions and for dipole transitions with  $\Delta J = 0$ . In assigning level spins and parities we have assumed that the stretched quadrupole transitions are of electric nature ( $E2$ ), while the  $\Delta I = 1$  transitions having  $R_{ADO}$  significantly different from 0.8 are mixed transitions of  $E2/M1$  type.

To derive the lifetimes by the Doppler-shift attenuation method line shapes were analyzed from the three asymmetric matrices created using the detectors in the rings at  $37^\circ$ ,  $90^\circ$ , and  $143^\circ$  on the first axis, and all detectors on the second axis. Spectra were generated by setting gates on the fully stopped transitions at the bottom of the bands of interest. The gates were chosen carefully to avoid contaminating transitions. Level lifetimes were extracted based on the shape analysis using the code LINESHAPE [37]. The slowing down history of the  $^{130}\text{La}$  recoils in the target and backing was simulated using Monte Carlo techniques and a statistical distribution was created for the projection of the recoil velocity with respect to the direction of the detected  $\gamma$  ray. Moreover, the kinematic effects of the nucleon evaporation were included, as well as the finite solid angle of the detectors. For the description of the electronic and nuclear scattering the Ziegler stopping powers [38,39] have been used. Extraction of lifetimes was done step by step, starting from the upper levels. At each level the intensity balance of feeding and decaying transitions was investigated allowing to establish the amount of side feeding from unobserved transitions. In a study devoted to lifetimes and side-feeding population of the yrast band levels in  $^{131}\text{La}$  using the  $^{122}\text{Sn}(^{14}\text{N}, 5n)$  reaction [40], spin-dependent effective side-feeding times were derived, with values ranging from  $\approx 0.06$  ps at spin around  $20\hbar$  to  $\approx 0.13$  ps at spin around  $13\hbar$  for the contribution from quasicontinuum levels. These values for the side-feeding times were adopted in the present work. To test the validity of this choice, we performed a DSAM analysis for the  $23/2^-$ ,  $27/2^-$ , and  $31/2^-$  states of the yrast negative-parity band in  $^{129}\text{La}$ , well populated in our experiment. The derived lifetimes were found in very good agreement with previously reported values [41], what gave confidence in the adopted procedure.

Lifetimes of excited states in the subnanosecond and nanosecond domains were investigated through in-beam measurements of triple- $\gamma$  coincidences using the array of HPGe and  $\text{LaBr}_3(\text{Ce})$  detectors. The procedure is presented in detail in Ref. [42]. Data were sorted into  $E_{\gamma 1}\text{--}E_{\gamma 2}\text{--}\Delta T$  cubes, where  $E_{\gamma 1}$  and  $E_{\gamma 2}$  represent the energy measured in the  $\text{LaBr}_3(\text{Ce})$  detectors, while  $\Delta T$  represents the time difference between the detection of the two  $\gamma$  rays. To further clean the cascade

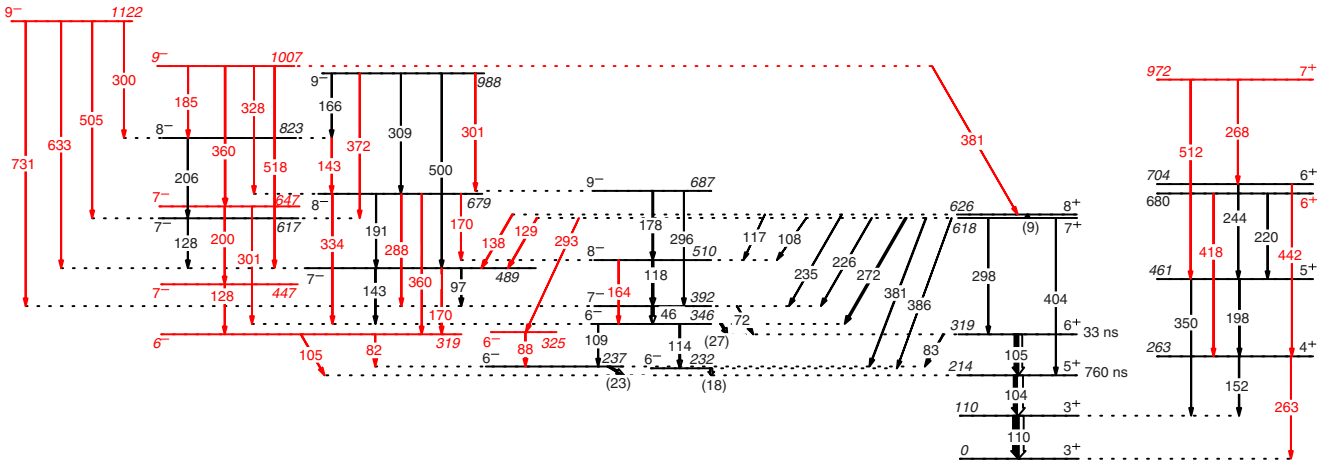


FIG. 1. Low-lying level scheme of  $^{130}\text{La}$  from Ref. [43] and present work. New levels and transitions are drawn with red color. The transitions between states of the same parity are shown as vertical arrows; the transitions connecting states of different parities are shown as tilted arrows. The arrows with energy labels in parentheses indicate unobserved tentative transitions.

of interest detected in the  $\text{LaBr}_3(\text{Ce})$  detectors, additional  $\gamma$  rays detected in the HPGe were used as a gate.

### III. EXPERIMENTAL RESULTS

#### A. Level scheme

Based on the observed  $\gamma$ - $\gamma$ -coincidence relations we have significantly extended the level scheme of  $^{130}\text{La}$ . The derived level scheme at low excitation energy and low- and medium-spin is illustrated in Fig. 1, while the high-spin band structures are shown in Figs. 2 and 3 for positive and negative parity, respectively. 100 new transitions and 45 new levels have been included.

The experimental information on the observed transitions is given in Table I. Illustrative coincidence spectra are shown in Fig. 4. Spins and parities of the new states have been assigned on the basis of multiplicities of their deexciting transitions deduced from the  $R_{ADO}$  values. Most transitions were assigned of pure dipole or quadrupole type (Table I). A few transitions were found as having a mixed dipole+quadrupole character.

The high-spin structures labeled as bands 1 and 2 have been reported in previous studies [29,30], however, without excitation energy and spin assignments. The decay out of these bands to the ground state has been elucidated in a work performed recently at IFIN-HH [43]. An excitation energy of 617.5 keV was established for the  $7^+$  band head of the yrast band 1, which exhibits a complex decay to the lower-lying positive- and negative-parity states. In the present study, two new weak transitions of 128.7 and 292.7 keV were added in the decay of the  $7^+$  band head feeding the known  $7^-$  488.8 keV state and a new  $6^-$  state at 324.8 keV, respectively (see Fig. 1). Moreover, a weak transition of 137.6 keV was included in the decay of the 626.4-keV  $8^+$  state of the band.

The low-lying positive-parity non-yrast structure identified in Ref. [43] has been confirmed and completed with several new transitions, up to spin  $7^+$  at 972.3 keV (Fig. 1). The spin of the 680.3-keV level, assigned as 5 in Ref. [43], has been

changed to 6, based on the  $R_{ADO}$  value of 0.84(9) derived for the 219.5-keV transition feeding the  $5^+$  level at 460.8 keV, and on the observation of a new 417.5-keV deexciting transition with  $R_{ADO} = 1.55(35)$ , that populates the  $4^+$  state at 263 keV.

The irregular level scheme of medium spin has been completed also on the negative-parity side. The states reported in Ref. [43] up to spin  $9^-$  at 988 keV have been confirmed and new transitions were added in their decay. Moreover six new states have been identified, namely two  $6^-$  states at 319- and 325-keV excitation energies, two  $7^-$  states at 489- and 647-keV excitation energies, and two states with  $J^\pi = 9^-$  at 1007- and 1122-keV excitation energies. The complex decay scheme of the new states has been elucidated. High-spin structures have been identified on top of the observed  $9^-$  states (see below).

From the energy-time matrix time spectra were created for transitions deexciting the low-lying levels, with the aim to search for longer-lived states. Excepting for the transitions deexciting the known  $5^+$  and  $6^+$  isomeric states reported in our previous work [43], in all investigated cases the time spectra showed only a prompt component, indicated lifetimes shorter than 15 ns.

As seen in Fig. 1, a new  $6^-$  state was placed at an energy of 319.2 keV. The spin of this state was assigned based on the characteristics of its feeding transitions, namely, the 360.1-keV quadrupole transition from the  $8^-$  679-keV state [ $R_{ADO} = 1.52(28)$ ], the 169.7-keV transition of mixed dipole/quadrupole character from the  $7^-$  489-keV state [ $R_{ADO} = 1.58(22)$ ], and the 128.2-keV dipole transition from the  $7^-$  447-keV level [ $R_{ADO} = 0.86(15)$ ]. The negative parity was established based on the  $E2$  multipolarity assigned to the 360.1-keV transition. An  $M2$  multipolarity for this transition was ruled out, as it would correspond, for a lifetime  $\tau < 15$  ns, to a transition strength  $B(M2)(360.1 \text{ keV}) > 3.5 \text{ W.u.}$ , higher than the upper limit of 1 W.u. recommended for this mass region [45]. The same argument was used in the case of the mixed dipole+quadrupole 169.7-keV transition, that was assigned as  $M1 + E2$ , giving additional support to the

TABLE I. Energies, relative intensities, ADO ratios, and multipolarities of  $\gamma$  rays assigned in the present work to  $^{130}\text{La}$ , as well as the band assignment for the initial state, the spin-parities of the initial and final states, and the excitation energy of the initial state for the decay.

$E_\gamma$ (keV)	$I_\gamma$	$R_{ADO}$	Multipolarities	Band	$J_i^\pi$	$J_f^\pi$	$E_i$ (keV)
82.4(2)	0.6(2)				$6^-$	$6^-$	319.2
82.5(2) <sup>a</sup>	9.9(8) <sup>b</sup>				$6^+$	$6^-$	319.1
86.1(2)	0.7(3)				$13^-$	$12^-$	2497.5
88.2(2)	1.8(5)				$6^-$	$6^-$	324.8
97.3(2)	3.9(3)	1.28(17)	$M1$		$7^-$	$7^-$	488.8
103.6(2) <sup>a</sup>	57.4(29) <sup>b</sup>		$E2$		$5^+$	$3^+$	214.0
105.1(2) <sup>a</sup>	61.8(36) <sup>b</sup>	0.85(8)	$M1$		$6^+$	$5^+$	319.1
105.2(2)	6.4(9)	0.87(9)	$E1$		$6^-$	$5^+$	319.2
108.0(2)	1.8(3)	0.87(14)	$E1$	1	$7^+$	$8^-$	617.5
109.1(2)	1.3(5)			2	$6^-$	$6^-$	345.7
110.4(2)	100(3) <sup>b</sup>		$M1$		$3^+$	$3^+$	110.4
113.7(2)	21.2(13)	1.34(13)	$M1$	2	$6^-$	$6^-$	345.7
116.9(2)	0.20(8)			1	$8^+$	$8^-$	626.4
118.0(2)	16.5(14)	0.75(5)	$M1$	2	$8^-$	$7^-$	509.5
127.9(2)	3.1(3)	1.41(23)	$M1$		$7^-$	$7^-$	616.7
128.2(2)	2.3(2)	0.86(15)	$M1$		$7^-$	$6^-$	447.4
128.6(3)	0.7(2)			1	$7^+$	$7^-$	617.5
130.3(2)	1.8(3)	0.82(5)	$M1$	9	$14^-$	$13^-$	2900.3
137.0(2)	27.4(14)	0.80(6)	$M1$	1	$10^+$	$9^+$	805.7
137.6(3)	1.0(3)	0.72(11)	$E1$	1	$8^+$	$7^-$	626.4
143.1(2)	3.5(3)	0.85(11)	$M1$		$7^-$	$6^-$	488.8
143.2(2)	0.9(2)	1.35(27)	$M1$		$8^-$	$8^-$	822.6
152.1(2)	6.1(9)	0.74(10)	$M1$		$4^+$	$3^+$	262.5
163.8(3)	0.35(9)	1.38(28)	$E2$	2	$8^-$	$6^-$	509.5
165.8(2)	1.1(3)			10	$9^-$	$8^-$	988.4
169.7(2)	1.8(4)	1.58(22)	$M1/E2$		$7^-$	$6^-$	488.8
169.9(2)	2.4(5)	1.42(23)	$M1$		$8^-$	$8^-$	679.4
177.5(2)	18.4(7)	0.83(5)	$M1$	2	$9^-$	$8^-$	687.0
179.1(3)	0.5(2)			1	$10^+$	$8^+$	805.7
184.7(3)	0.25(8)			11	$9^-$	$8^-$	1007.1
186.7(3)	0.6(2)	0.77(19)	$M1$	5	$8^+$	$9^+$	855.4
190.6(2)	3.6(4)	0.56(9)	$M1/E2$		$8^-$	$7^-$	679.4
198.3(2)	3.4(7)	0.79(8)	$M$		$5^+$	$4^+$	460.8
199.8(2)	2.1(3)	1.45(20)	$M1$		$7^-$	$7^-$	647.2
205.9(2)	1.5(2)	0.81(8)	$M1$		$8^-$	$7^-$	822.6
219.5(2)	1.0(2)	0.84(9)	$M1$		$6^+$	$5^+$	680.3
220.9(2)	9.6(4)	0.72(5)	$M1$	2	$10^-$	$9^-$	907.9
221.6(3)	0.5(2)	0.85(18)	$M1$	5	$9^+$	$8^+$	1077.0
226.0(2)	6.6(5)	1.45(9)	$E1$	1	$7^+$	$7^-$	617.5
234.9(2)	6.2(6)	0.81(5)	$E1$	1	$8^+$	$7^-$	626.4
237.9(3)	0.7(2)	0.77(15)	$M1$	5	$8^+$	$7^+$	855.4
239.0(2)	0.35(8)	0.66(8)	$M1$		$15^-$	$14^-$	3216.4
242.3(2)	2.8(3)	0.85(4)	$M1$	9	$15^-$	$14^-$	3142.6
243.6(2)	1.1(3)	0.81(6)	$M1$		$6^+$	$5^+$	704.4
245.9(2)	15.9(13)	0.80(4)	$M1$	1	$12^+$	$11^+$	1330.7
262.4(2)	0.34(9)				$4^+$	$3^+$	262.5
267.9(2)	0.55(19)	0.85(15)	$M1$		$7^+$	$6^+$	972.3
269.5(2)	7.6(5)	0.71(5)	$M1$	2	$11^-$	$10^-$	1177.4
271.3(3)	0.9(3)			5	$9^+$	$10^+$	1077.0
271.8(2)	25.2(13)	0.82(5)	$E1$	1	$7^+$	$6^-$	617.5
279.1(2)	26.6(14)	0.80(5)	$M1$	1	$11^+$	$10^+$	1084.8
282.0(2)	1.2(3)	0.83(11)	$M1$	5	$11^+$	$10^+$	1651.2
284.4(2)	0.6(2)	0.84(12)	$M1$	5	$10^+$	$11^+$	1369.2
287.7(2)	1.1(2)	0.78(14)	$M1$		$8^-$	$7^-$	679.4
292.2(2)	1.24(25)	0.71(14)	$M1$	5	$10^+$	$9^+$	1369.2
292.7(2)	1.8(4)	0.85(9)	$E1$	1	$7^+$	$6^-$	617.5

TABLE I. (Continued.)

$E_\gamma$ (keV)	$I_\gamma$	$R_{ADO}$	Multipolarities	Band	$J_i^\pi$	$J_f^\pi$	$E_i$ (keV)
295.5(2)	3.2(6)	1.38(18)	$E2$	2	$9^-$	$7^-$	687.0
298.4(2)	2.9(11)	0.87(11)	$M1$	1	$7^+$	$6^+$	617.5
299.2(3)	0.7(2)				$9^-$	$8^-$	1122.1
301.3(2)	1.9(2)	0.84(8)	$M1$		$7^-$	$6^-$	647.2
301.4(2)	0.3(1)			10	$9^-$	$9^-$	988.4
303.0(2)	6.0(5)	0.70(5)	$M1$	2	$12^-$	$11^-$	1480.4
303.4(3)	0.8(3)	0.85(6)	$M1$	6	$11^+$	$10^+$	1780.1
309.0(2)	1.3(3)	0.48(10)	$M1/E2$	10	$9^-$	$8^-$	988.4
313.4(3)	1.4(4)	0.72(11)	$M1$	6	$12^+$	$11^+$	2093.5
313.5(3)	0.2(1)	0.92(22)	$M1$	5	$12^+$	$13^+$	2018.5
313.9(2)	2.4(2)	0.80(7)	$M1$	9	$16^-$	$15^-$	3456.5
320.7(3)	0.29(12)	0.86(10)	$M1$	5	$11^+$	$12^+$	1651.2
326.0(2)	6.4(19)	0.81(4)	$M1$	1	$14^+$	$13^+$	2031.0
327.7(3)	0.8(3)	0.47(6)	$M1/E2$	11	$9^-$	$8^-$	1007.1
331.5(4)	0.2(1)			6	$10^+$	$9^+$	1476.7
333.7(2)	2.8(5)	1.51(25)	$E2$		$8^-$	$6^-$	679.4
343.2(3)	0.9(2)	0.67(9)	$M1$	3	$13^+$	$12^+$	2060.6
346.9(2)	3.4(5)	0.63(6)	$M1/E2$	2	$13^-$	$12^-$	1827.4
350.4(3)	1.2(3)				$5^+$	$3^+$	460.8
356.5(4)	2.5(4)	0.71(5)	$M1$	3	$12^+$	$11^+$	1717.3
358.6(3)	3.2(5)	0.61(6)	$M1/E2$	9	$13^-$	$12^-$	2770.0
359.9(3)	2.9(3)	1.55(25)	$E2$	11	$9^-$	$7^-$	1007.1
360.1(3)	2.3(5)	1.52(28)	$E2$		$8^-$	$6^-$	679.4
367.3(3)	1.18(25)	0.65(14)	$M1$	5	$12^+$	$11^+$	2018.5
371.2(9)	0.90(21)	0.75(16)	$M1$	3	$16^+$	$15^+$	3243.0
371.6(6)	1.8(3)	0.76(7)	$M1$	9	$17^-$	$16^-$	3828.1
371.7(2)	0.5(1)			10	$9^-$	$7^-$	988.4
373.1(2)	1.3(2)	0.59(8)	$M1/E2$	2	$14^-$	$13^-$	2200.4
374.3(2)	11.3(22)	0.78(4)	$M1$	1	$13^+$	$12^+$	1705.0
375.4(2)	3.5(4)	1.75(35)	$E2$	7	$11^{(+)}$	$9^{(+)}$	1557.0
375.9(3)	2.9(4)			7	$9^{(+)}$	$10^+$	1181.6
380.8(3)	0.22(9)			11	$9^-$	$8^+$	1007.1
380.9(2)	9.5(11)	0.78(9)	$E1$	1	$7^+$	$6^-$	617.5
384.8(3)	1.13(17)	0.78(12)	$M1$	3	$14^+$	$13^+$	2445.4
385.4(8)	0.18(7)			3	$18^+$	$17^+$	4120.5
385.5(2)	0.60(24)			1	$7^+$	$6^-$	617.5
392.8(2)	2.7(8)	0.77(6)	$M1$	1	$16^+$	$15^+$	2869.3
398.4(2)	3.8(8)	1.42(9)	$E2$	2	$10^-$	$8^-$	907.9
399.7(3)	1.15(18)	0.61(6)	$M1/E2$	6	$10^+$	$9^+$	1476.7
402.8(3)	1.0(2)	0.63(5)	$M1/E2$	9	$14^-$	$13^-$	2900.3
403.5(2)	3.3(9)	1.34(13)	$E2$	1	$7^+$	$5^+$	617.5
410.9(3)	0.52(17)			6	$11^+$	$10^+$	1780.1
411.3(4)	0.44(13)	0.71(11)	$M1$	5	$13^+$	$12^+$	2429.8
414.1(4)	0.13(5)			4	$15^+$	$14^+$	3028.4
414.6(2)	0.9(3)	0.48(7)	$M1/E2$	2	$15^-$	$14^-$	2615.0
416.1(2)	2.5(5)	1.49(21)	$E2$	1	$11^+$	$9^+$	1084.8
417.7(3)	0.5(2)	1.55(35)	$E2$		$6^+$	$4^+$	680.3
423.5(3)	1.1(3)	0.72(7)	$M1$	9	$18^-$	$17^-$	4251.6
426.2(4)	1.36(31)	0.80(10)	$M1$	3	$15^+$	$14^+$	2872.3
433.5(4)	0.39(15)	0.65(9)	$M1/E2$	2	$16^-$	$15^-$	3048.5
434.5(3)	1.1(4)	0.76(9)	$M1$	4	$14^+$	$13^+$	2614.3
441.9(3)	0.95(32)	1.33(25)	$E2$		$6^+$	$4^+$	704.4
445.2(7)	0.9(3)	0.75(13)	$M1$	1	$18^+$	$17^+$	3824.4
445.5(3)	6.4(17)	0.78(9)	$M1$	1	$15^+$	$14^+$	2476.5
448.8(3)	0.38(14)			2	$20^-$	$19^-$	4950.3
450.6(3)	1.3(3)	0.75(15)	$M1$	5	$9^+$	$8^+$	1077.0
462.5(3)	2.0(2)	0.51(8)	$M1/E2$	4	$13^+$	$12^+$	2179.8

TABLE I. (*Continued.*)

$E_\gamma$ (keV)	$I_\gamma$	$R_{ADO}$	Multipolarities	Band	$J_i^\pi$	$J_f^\pi$	$E_i$ (keV)
464.8(5)	0.6(2)	0.57(9)	$M1/E2$	2	$21^-$	$20^-$	5415.1
464.9(5)	0.85(25)	0.73(8)	$M1$	9	$19^-$	$18^-$	4716.5
469.8(5)	0.38(16)	0.61(9)	$M1/E2$	2	$17^-$	$16^-$	3519.6
481.5(5)	0.2(1)			2	$18^-$	$17^-$	4001.5
486.0(8)	0.5(2)			1	$20^+$	$19^+$	4873.5
490.4(2)	8.9(5)	1.42(9)	$E2$	2	$11^-$	$9^-$	1177.4
492.3(6)	0.82(18)	0.65(9)	$M1$	3	$17^+$	$16^+$	3735.3
499.6(4)	3.4(4)	1.51(15)	$E2$	10	$9^-$	$7^-$	988.4
499.8(5)	0.15(7)			2	$19^-$	$18^-$	4501.7
503.0(5)	0.48(11)	0.76(9)	$M1$	9	$20^-$	$19^-$	5219.5
505.1(3)	0.5(2)	1.36(25)	$E2$		$9^-$	$7^-$	1122.1
509.9(6)	2.7(7)	0.66(13)	$M1$	1	$17^+$	$16^+$	3378.7
511.7(4)	1.0(4)	1.51(31)	$E2$		$7^+$	$5^+$	972.3
514.0(3)	0.12(6)			5	$10^+$	$8^+$	1369.2
518.3(3)	1.1(2)	1.36(12)	$E2$	11	$9^-$	$7^-$	1007.1
518.5(3)	0.9(2)	0.54(9)	$M1/E2$	6	$9^+$	$8^+$	1144.9
525.0(3)	9.5(11)	1.36(8)	$E2$	1	$12^+$	$10^+$	1330.7
533.1(5)	0.25(8)	0.85(15)	$M1$	9	$21^-$	$20^-$	5752.6
535.3(4)	3.7(4)	1.38(7)	$E2$	11	$11^-$	$9^-$	1542.4
550.0(3)	2.6(3)	1.42(8)	$E2$	7	$13^{(+)}$	$11^{(+)}$	2107.0
554.0(3)	2.8(4)	1.38(7)	$E2$	11	$11^-$	$9^-$	1542.4
555.1(3)	3.5(4)	0.55(5)	$M1/E2$	3	$11^+$	$10^+$	1360.8
555.2(3)	0.8(2)	0.78(11)	$D$	7	$9^{(+)}$	$8^+$	1181.6
564.0(6)	0.5(2)	0.75(15)	$M1$	1	$19^+$	$18^+$	4388.9
572.5(2)	11.1(7)	1.46(12)	$E2$	2	$12^-$	$10^-$	1480.4
574.0(3)	0.17(8)			5	$11^+$	$9^+$	1651.2
574.8(3)	1.8(3)	0.45(9)	$M1/E2$	8	$(8)^+$	$7^+$	1192.3
584.0(3)	3.4(5)	0.98(9)	$M1/E2$		$12^-$	$13^-$	2411.4
614.8(4)	1.8(4)	1.38(10)	$E2$	10	$11^-$	$9^-$	1621.9
620.2(3)	4.5(12)	1.47(10)	$E2$	1	$13^+$	$11^+$	1705.0
632.4(3)	2.0(4)	0.47(6)	$M1/E2$	3	$12^+$	$11^+$	1717.3
633.3(3)	1.0(2)	1.53(21)	$E2$		$9^-$	$7^-$	1122.1
633.5(3)	3.0(4)	1.38(12)	$E2$	10	$11^-$	$9^-$	1621.9
634.8(4)	0.4(1)	0.78(13)	$M1$	11	$11^-$	$10^-$	1542.4
649.6(4)	0.6(2)	1.45(38)	$E2$	5	$12^+$	$10^+$	2018.5
650.0(3)	8.7(10)	1.45(10)	$E2$	2	$13^-$	$11^-$	1827.4
653.5(4)	1.0(2)	1.35(15)	$E2$	8	$(10)^+$	$(8)^+$	1845.8
692.1(4)	0.8(2)	1.36(18)	$E2$	3	$11^+$	$9^+$	1360.8
695.6(5)	5.7(9)	1.32(9)	$E2$	11	$13^-$	$11^-$	2238.0
699.9(4)	0.89(14)	1.32(18)	$E2$	3	$13^+$	$11^+$	2060.6
700.3(2)	9.4(23)	1.53(8)	$E2$	1	$14^+$	$12^+$	2031.0
700.8(4)	1.5(2)	1.50(15)	$E2$	7	$15^{(+)}$	$13^{(+)}$	2807.8
709.3(4)	1.1(2)				$11^-$	$9^-$	1831.4
714.2(5)	0.3(1)			10	$11^-$	$10^-$	1621.9
720.0(4)	7.9(8)	1.45(7)	$E2$	2	$14^-$	$12^-$	2200.4
724.8(5)	0.34(12)			5	$13^+$	$13^+$	2429.8
726.9(5)	1.0(2)	1.34(11)	$E2$	10	$13^-$	$11^-$	2348.8
728.4(6)	0.63(14)	1.44(6)	$E2$	3	$14^+$	$12^+$	2445.4
729.9(6)	1.6(3)	0.56(6)	$M1/E2$	3	$13^+$	$12^+$	2060.6
730.5(4)	0.3(1)				$9^-$	$7^-$	1122.1
739.4(3)	0.45(9)	0.65(9)	$M1$		$14^-$	$13^-$	2977.4
740.4(3)	1.08(25)	0.52(6)	$M1/E2$	3	$14^+$	$13^+$	2445.4
766.0(7)	0.57(18)	0.65(8)	$M1/E2$	3	$16^+$	$15^+$	3243.0
771.4(4)	4.6(11)	1.52(9)	$E2$	1	$15^+$	$13^+$	2476.5
774.0(10)	0.3(1)	1.45(42)	$E2$	8	$(12)^+$	$(10)^+$	2619.8
778.9(6)	0.22(10)			5	$13^+$	$11^+$	2429.8
787.6(4)	5.5(8)	1.41(7)	$E2$	2	$15^-$	$13^-$	2615.0

TABLE I. (Continued.)

$E_\gamma$ (keV)	$I_\gamma$	$R_{ADO}$	Multipolarities	Band	$J_i^\pi$	$J_f^\pi$	$E_i$ (keV)
789.7(5)	0.4(2)	0.69(12)	$M1$		$12^-$	$11^-$	2411.4
790.2(6)	0.5(2)	1.45(15)	$E2$	10	$15^-$	$13^-$	3139.0
797.6(5)	1.83(20)	1.39(9)	$E2$	3	$16^+$	$14^+$	3243.0
808.6(6)	1.6(4)	1.33(10)	$E2$	11	$15^-$	$13^-$	3046.6
811.7(6)	1.72(22)	1.33(13)	$E2$	3	$15^+$	$13^+$	2872.3
832.6(6)	0.3(1)	1.40(25)	$E2$	10	$15^-$	$13^-$	3181.4
838.2(6)	0.8(2)	1.36(14)	$E2$	7	$17^{(+)}$	$15^{(+)}$	3646.0
838.3(5)	8.8(22)	1.43(9)	$E2$	1	$16^+$	$14^+$	2869.3
841.9(9)	0.36(14)			3	$15^+$	$14^+$	2872.3
843.2(6)	0.5(2)				$11^-$	$9^-$	1831.4
848.1(5)	3.9(7)	1.43(12)	$E2$	2	$16^-$	$14^-$	3048.5
848.6(6)	0.28(5)	1.49(29)	$E2$	4	$15^+$	$13^+$	3028.4
863.0(6)	1.08(24)	1.45(25)	$E2$	3	$17^+$	$15^+$	3735.3
876.4(8)	0.3(1)	1.55(29)	$E2$		$13^-$	$11^-$	2497.5
877.5(8)	1.48(18)	1.44(23)	$E2$	3	$18^+$	$16^+$	4120.5
902.2(6)	3.3(7)	1.53(11)	$E2$	1	$17^+$	$15^+$	3378.7
904.6(6)	3.2(6)	1.42(9)	$E2$	2	$17^-$	$15^-$	3519.6
906.6(6)	0.9(3)	1.35(13)	$E2$	11	$17^-$	$15^-$	3953.2
913.0(8)	0.6(2)			2	$21^-$	$19^-$	5415.1
934.1(5)	0.9(3)	0.72(9)	$M1$	5	$12^+$	$11^+$	2018.5
938.6(6)	0.9(2)	1.37(13)	$E2$	9	$13^-$	$11^-$	2770.0
948.8(6)	1.20(35)			2	$20^-$	$18^-$	4950.3
953.0(6)	1.27(36)	1.50(17)	$E2$	2	$18^-$	$16^-$	4001.5
955.1(6)	3.9(7)	1.37(7)	$E2$	1	$18^+$	$16^+$	3824.4
957.0(10)	0.45(13)	1.41(17)	$E2$	7	$19^{(+)}$	$17^{(+)}$	4603.0
967.2(10)	0.11(4)			9	$20^-$	$18^-$	5219.5
978.7(7)	0.10(5)				$15^-$	$13^-$	3216.4
982.1(9)	1.0(3)	1.29(14)	$E2$	2	$19^-$	$17^-$	4501.7
1010.2(8)	1.6(4)			1	$19^+$	$17^+$	4388.9
1049.1(8)	2.4(7)			1	$20^+$	$18^+$	4873.5
1234.4(8)	1.0(3)				$12^-$	$11^-$	2411.4

<sup>a</sup>Isomeric transitions (Ref. [43]).

<sup>b</sup>Intensity derived from single spectra (Refs. [43,44]). In the case of the 82.5- and 105.1-keV transitions, the contribution from the 82.4- and 105.2-keV transitions, respectively, has been subtracted.

negative parity. The 319 keV  $6^-$  state decays by a transition of 105.2 keV [ $R_{ADO} = 0.87(9)$ ] and a weak transition of 82.4 keV, feeding the yrast  $5^+$  state lying at 214-keV excitation energy and the  $6^-$  state lying at 237-keV excitation energy, respectively. It is worthwhile to mention that the  $6^-$  state at 319.2 keV is just 0.1 keV apart from the known yrast  $6^+$  state. Moreover the two states decay by transitions with almost identical energies. Note however that the intensity ratio  $I(82 \text{ keV})/I(105 \text{ keV})$  differs in the two states, having values of 0.160(15) and 0.094(34) for the  $6^+$  and  $6^-$  states, respectively. This finding stands as a direct evidence of the existence of two different states at 319-keV excitation energy.

The positive-parity band 1 was observed in the present experiment up to spin value  $20\hbar$ . A weak transition of 179.3 keV has been placed between the  $10^+$  and  $8^+$  states at the bottom of the band. Band 3, proposed in Ref. [33], has been confirmed and extended by two more states, with spins  $17^+$  and  $18^+$ , based on the observation of the  $E2$  transitions of 863.0 and 877.5 keV. Five new transitions, with energies of 343.4, 385.2, 492.3, 863.0, and 877.5 keV, were included in

this band. A new 692.3-keV transition with  $R_{ADO} = 1.36(18)$  was found to link the  $11^+$  state with the  $9^+$  state of the yrast band.

A short sequence of positive-parity levels, labeled as band 4, was identified to be connected with band 3. Spin and parity  $13^+$  for its lowest state were assigned based on the  $M1 + E2$  mixed character of the 463-keV deexciting transition [ $R_{ADO} = 0.51(8)$ ] to the  $12^+$  state of band 3. Band 5 is a new structure of states with spins from  $8^+$  to  $13^+$  connected by  $M1$  transitions and very weak  $E2$  transitions. Besides in-band transitions, all states of this band decay to the states of band 1. A structure of weakly populated states connected by  $M1$  transitions was assigned as band 6. The spin-parity  $9^+$  of its band head was established as it decays by the mixed  $M1/E2$  518.5-keV transition [ $R_{ADO} = 0.54(9)$ ] to the  $8^+$  state of band 1.

The new band 7 was identified as a sequence of states connected by the 375.4-, 550.0-, 700.8-, 838.2-, and 957.0-keV quadrupole transitions. The band is deexcited by the 375.9- and 555.2-keV transitions towards the  $10^+$  and  $8^+$  states of

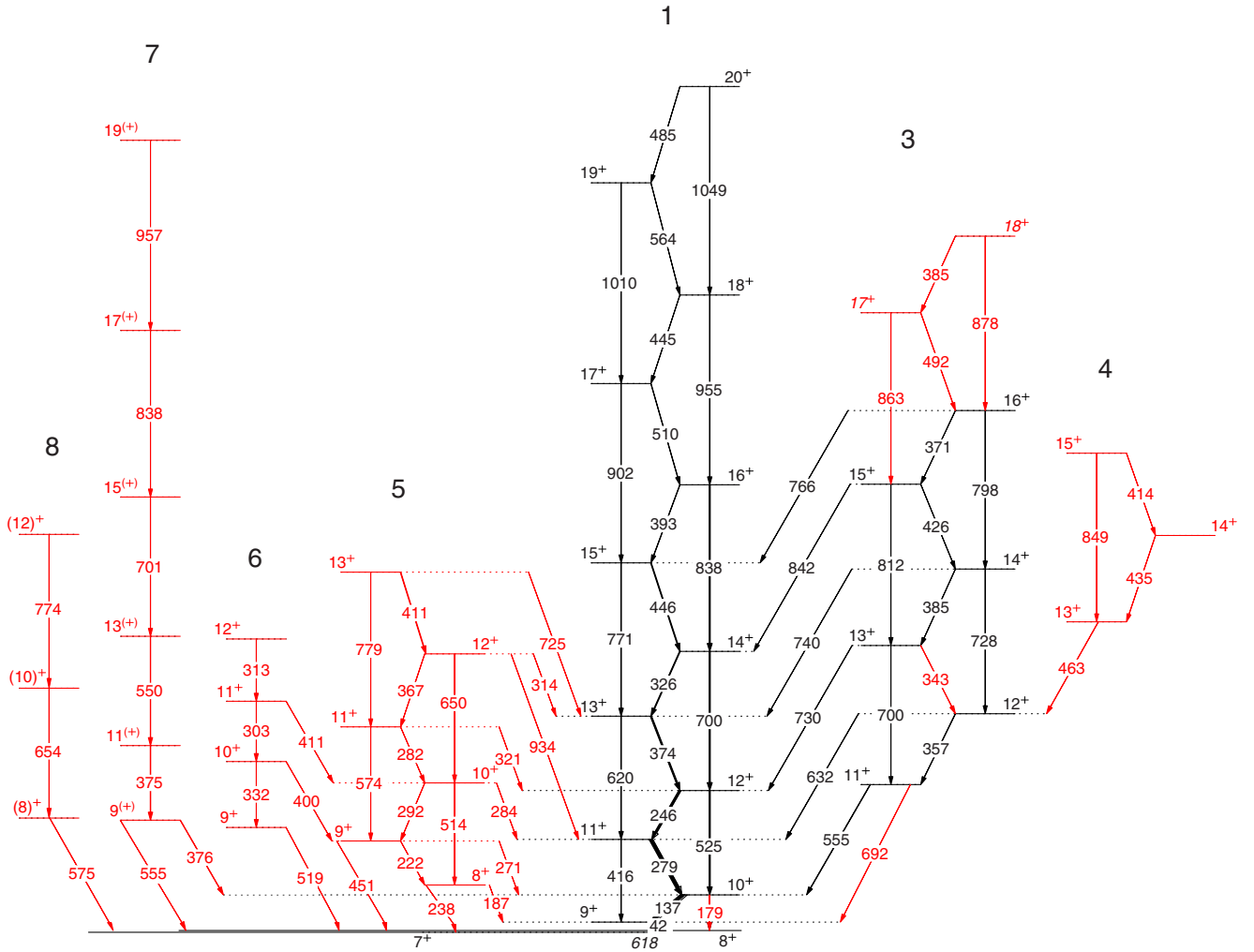


FIG. 2. Positive-parity bands of  $^{130}\text{La}$  from Ref. [43] and present work. New levels and transitions are drawn with red color. The lowest level shown is the  $7^+$  bandhead of band 1 with  $E_x = 618$  keV.

band 1, respectively. Figure 4(a) shows a sum of double-gated spectra obtained from the  $\gamma$ - $\gamma$ - $\gamma$  cube, which illustrates the  $\gamma$  lines of band 7, as well as the transitions known in the decay of band 1. A spin  $9\hbar$  was assigned to the band head based on the pure dipole character of the 555.2-keV transition [ $R_{ADO} = 0.78(11)$ ] feeding the  $8^+$  state of band 1. The parity could not be, however, assigned, as the 555.2-keV transition may have either an  $M1$  or an  $E1$  character. The positive parity tentatively assigned (in parentheses) is supported by theoretical considerations (see Sec. IV).

A structure composed of three states connected by the 653.5- and 774.0-keV  $E2$  transitions was assigned as belonging to the new rotational band 8. It is deexcited by the 574.8-keV transition that is coincident with transitions from the decay of band 1. Based on the mixed  $E2/M1$  type established for this transition [ $R_{ADO} = 0.45(9)$ ], a positive parity was assigned to the band. However, the excitation energy and the spin of the band head could not be assigned unambiguously, as the 574.8-keV decaying transition may be placed on either the  $8^+$  state or the  $7^+$  state at the bottom of band 1. In our proposed level scheme, the 574.8-keV transition was

placed to feed the  $7^+$  state and thus a spin 8 was assigned to the band head (see the discussion of Sec. IV).

On the negative-parity side, previously reported band 2 [29,30] was observed up to spin  $21\hbar$ . Note that in Ref. [30], by using the reaction  $^{51}\text{V}(^{82}\text{Se}, 3n)^{130}\text{La}$  at an energy of 290 MeV, six more states at high energies have been reported, but their absolute energies could not be fixed. In our previous paper (Ref. [43]) the band head was established at an excitation energy of 345.7 keV with  $J^\pi = 6^-$ . In the present work, a weak transition of 163.8 keV was included between the  $8^-$  and  $6^-$  states of the band. As seen in Table I, for  $J = 13-17$  and  $J = 21$  the deexciting  $\Delta J = 1$  transitions have  $R_{ADO}$  values around 0.6, somewhat smaller than the values corresponding to pure dipole transitions. Comparison of the experimental  $R_{ADO}$  ratios with the values calculated by assuming a Gaussian distribution of magnetic substates with  $\sigma/J \approx 0.3$ , indicated small mixing ratios of  $\delta \approx -0.2$ .

Band 9 consists of a sequence of nine states connected by dipole transitions. The corresponding  $R_{ADO}$  values indicated pure transitions. This structure has been previously reported in Ref. [31], however, without linking with the known states of

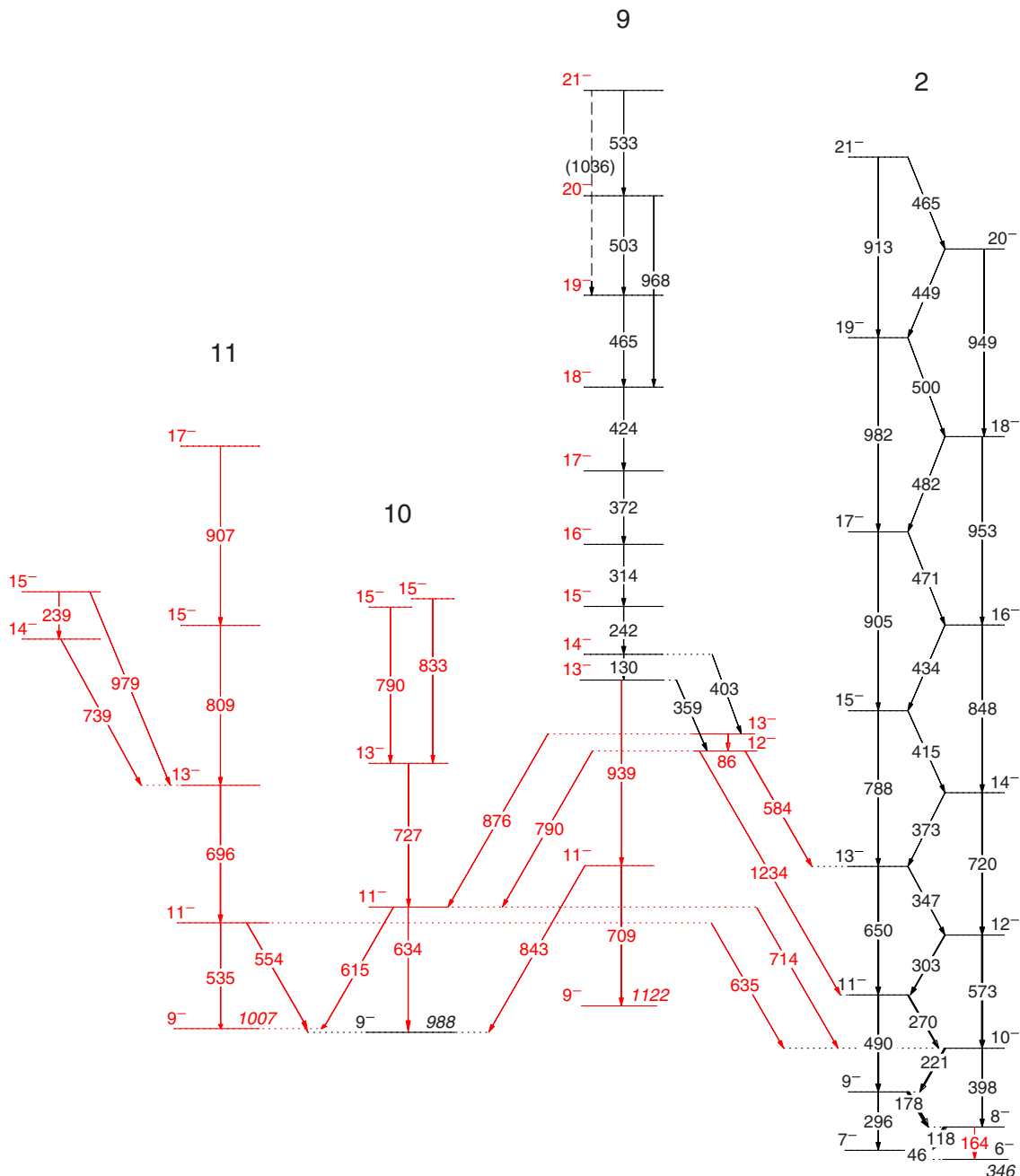


FIG. 3. Negative-parity bands of  $^{130}\text{La}$ . New levels and transitions are drawn with red color. The energy of the lowest-lying state of each observed structure is given to show the connection with the lower-lying states of Fig. 1. The transition of 1036 keV from the  $21^-$  state of band 9, shown as dotted arrow, was not seen in the present work, but was included according to Ref. [31].

$^{130}\text{La}$ , and therefore without spin and parity assignment. In the present study the decay out of this band has been elucidated. A spin-parity  $13^-$  was assigned to the band head placed at an excitation energy of 2770.0 keV. The transitions of 359 and 403 keV, reported in Ref. [31] to deexcite the band, were found in coincidence with the new transitions of 584 and 1234 keV that are feeding states of band 2. In addition, the in-band transitions were found in coincidence with the  $E2$  transitions of 939 and 709 keV, placed in cascade and feeding the  $9^-$  1122-keV state. Note that in Ref. [31] four more high-energy

states have been identified, and weak  $E2$  transitions were seen to deexcite states with spins  $J \geq 20$ . In our experiment we observed the weak 967-keV transition between the  $20^-$  and  $18^-$  states of the band. The  $E2$  transition from the  $21^-$  state was too weak to be observed, and is shown as dotted in Fig. 3. A coincidence spectrum obtained from the symmetric  $\gamma$ - $\gamma$  matrix gated by a sum of  $\gamma$  rays in the band is illustrated in Fig. 4(b).

Two weakly populated sequences of negative-parity states connected by  $E2$  transitions were labeled as bands 10 and

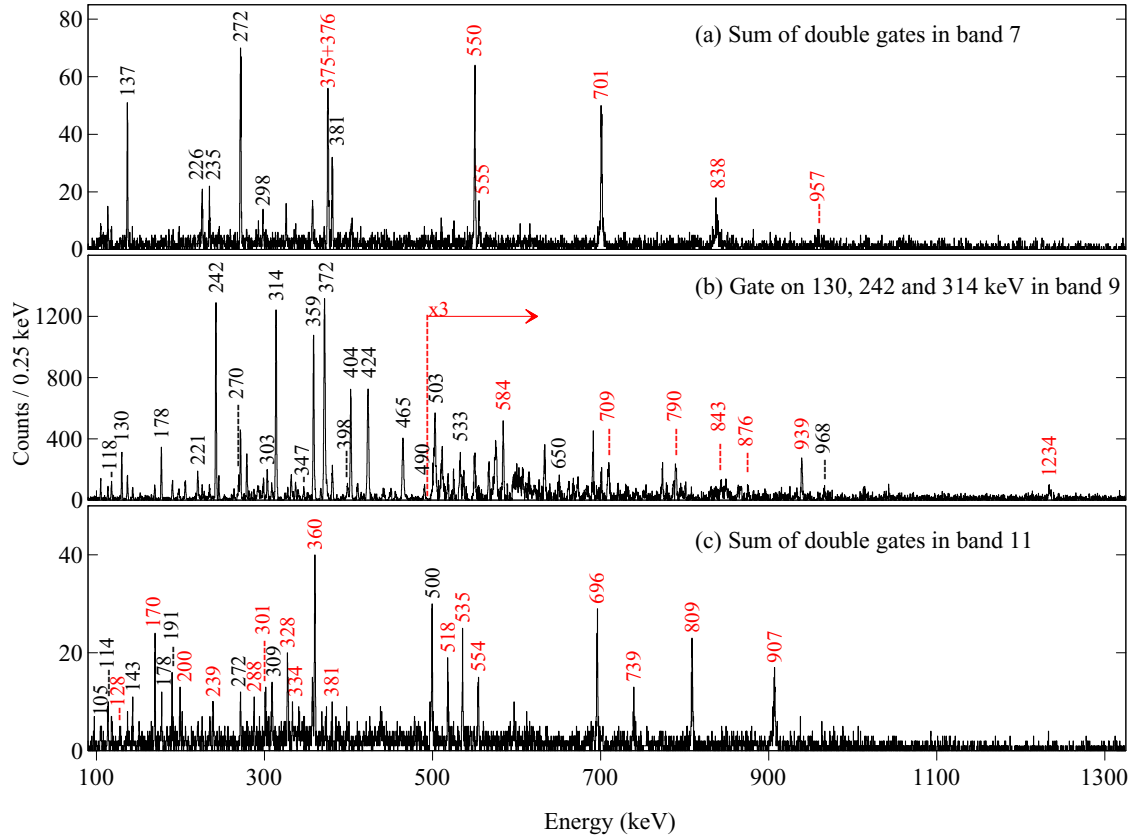


FIG. 4. (a) Sum of double-gated spectra in band 7 (375 + 555 keV, 375 + 376 keV, 550 + 376 keV, 550 + 555 keV) obtained from the  $\gamma - \gamma - \gamma$  cube; (b) Coincidence spectrum from the symmetric  $\gamma - \gamma$  matrix gated by transitions in band 9; (c) Sum of double-gated spectra in band 11 (696 + 535 keV, 696 + 554 keV, 696 + 809 keV, 554 + 809 keV, 535 + 809 keV) obtained from the  $\gamma - \gamma - \gamma$  cube. In all spectra, transitions belonging to the bands or involved in the decay of the bands are marked by energy. The new transitions are marked in red.

11 (Fig. 3). They are built on the  $9^-$  states at the excitation energies of 988 and 1007 keV. A sum of double-gated spectra obtained from the  $\gamma - \gamma - \gamma$  cube, which shows the  $\gamma$  lines of band 11, is given in Fig. 4(c). In the coincidence spectrum are also present the transitions from the complex decay of the  $9^-$  states (see Fig. 1), as well as the 239- and 739-keV  $\gamma$  lines that belong to a higher-spin structure connected to band 11 (see Fig. 3).

By using the reaction  $^{51}\text{V}(^{82}\text{Se}, 3n)^{130}\text{La}$  at a bombarding energy of 290 MeV, Godfrey *et al.* [32] reported the observation of nine transitions with energies of 762, 852, 920, 998, 1073, 1148, 1229, and 1319 keV, assigned to a highly deformed band with  $\beta_2 \approx 0.4$  and spins up to around  $34\hbar$ . The  $\gamma$  rays belonging to the highly deformed band were not seen in the present experiment. The  $^{121}\text{Sb}(^{12}\text{C}, 3n)^{130}\text{La}$  reaction used in our study was indeed efficient in populating spins in the range  $10 - 20\hbar$ , while the more symmetric  $^{51}\text{V}(^{82}\text{Se}, 3n)^{130}\text{La}$  reaction employed in Refs. [30–32] was appropriate for the population of higher-spin states.

### B. Lifetimes derived by Doppler-shift attenuation method

By applying the Doppler-shift attenuation method, lifetimes were derived for excited states in the positive-parity bands 1, 3, and 7, and in all negative-parity bands. As already mentioned, the lifetimes and the corresponding reduced

transition probabilities deduced for the chiral doublet partners (bands 1 and 3) were reported and discussed in a previous paper [34].

In the case of band 2, the analysis was performed for the  $E2$  deexciting transitions, as the  $M1$  transitions are much weaker. Line shapes were observed and analyzed for the levels with  $J^\pi = 14^-$  to  $17^-$  and  $21^-$ . The energies of transitions deexciting the  $18^-$  and  $20^-$  states are very close, and the corresponding line shapes were superimposed. This fact prevented assigning distinct lifetimes to the corresponding states. In the case of the transition deexciting the  $19^-$  level, a reliable analysis could not be done due to the presence of contaminants. In band 9, line shapes were analyzed for the  $M1$  deexciting transitions for states with spin parity from  $16^-$  to  $21^-$ . As concerns the quadrupole bands 7, 10, and 11, line shapes were observed for states with spin  $\geq 15$ . Examples of experimental line shapes and the corresponding fits are illustrated in Figs. 5, 6, and 7. The derived lifetimes are collected in Table II. Assigned errors include the uncertainties due to the stopping power calculation (10%) and to the side-feeding pattern (15%).

### C. Lifetime measurements with fast-timing technique

The lifetimes of lower-lying states in  $^{130}\text{La}$  have been investigated by using the fast-timing technique. For this

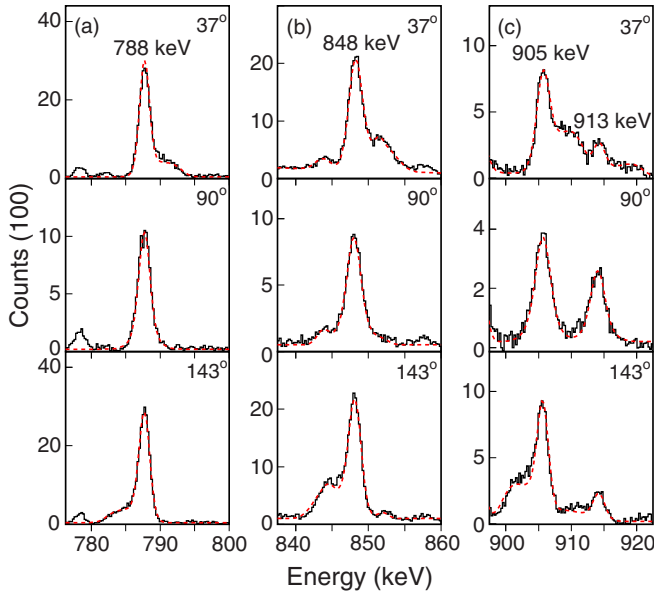


FIG. 5. Experimental and calculated line shapes for transitions deexciting the states in the band 2 of  $^{130}\text{La}$  with (a)  $J^\pi = 15^-$ , (b)  $16^-$ , (c)  $17^-$ , and (d)  $21^-$ , respectively. The coincidence spectra were created with narrow gates on lower-lying transitions emitted from stopped nuclei. The fitted DSAM spectra are shown in red dashed lines.

purpose, feeding and deexciting transitions were selected for the levels of interest, and corresponding time difference spectra were created. To clean the coincidence spectra appropriate gates were chosen in the HPGe spectra.

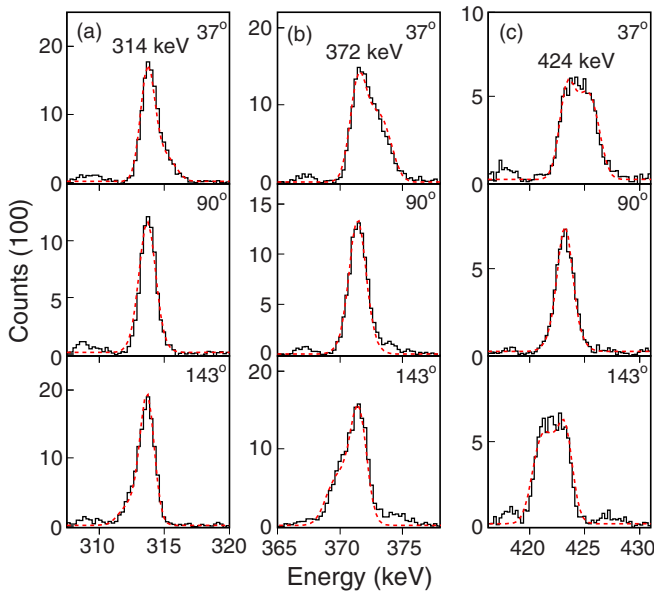


FIG. 6. Experimental and calculated line shapes for transitions deexciting the states in the band 9 of  $^{130}\text{La}$  with (a)  $J^\pi = 16^-$ , (b)  $17^-$ , and (c)  $18^-$ , respectively. The coincidence spectra were created with narrow gates on lower-lying transitions emitted from stopped nuclei. The fitted DSAM spectra are shown in red dashed lines.

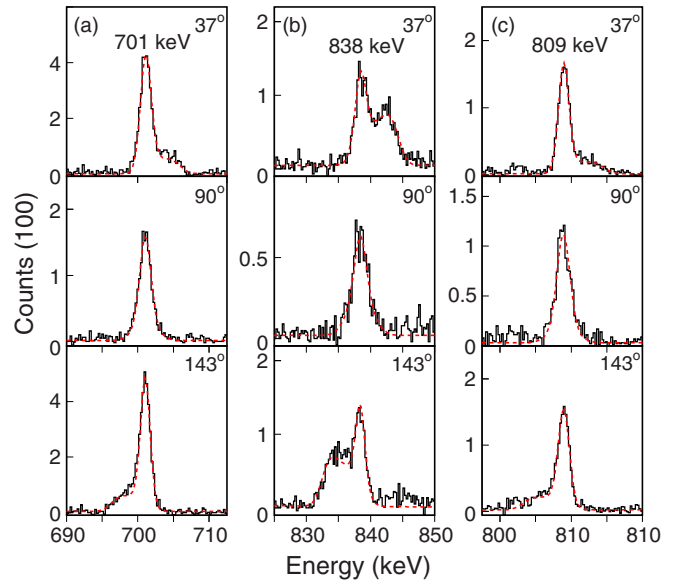


FIG. 7. Experimental and calculated lineshapes for transitions deexciting the states with (a)  $J^\pi = 15^+$  and (b)  $17^+$  in band 7, and (c)  $15^-$  in band 11. The coincidence spectra were created with narrow gates on lower-lying transitions emitted from stopped nuclei. The fitted DSAM spectra are shown in red dashed lines.

In a detailed analysis devoted to the positive-parity yrast band, the centroid method [42] has been used. Lifetimes of the lowest-lying states have been derived as  $\tau(8^+) = 120^{+20}_{-40}$  ps and  $\tau(10^+) < 30$  ps. The  $7^+$  band head of the band was

TABLE II. Lifetimes determined in the present work by applying the Doppler-shift attenuation method.

$E_x$ (keV)	$J^\pi$	$\tau$ (ps)
<b>Band 2</b>		
2200.4	$14^-$	2.11(51)
2615.0	$15^-$	1.12(22)
3048.5	$16^-$	0.76(14)
3519.6	$17^-$	0.55(12)
5415.1	$21^-$	0.45(13)
<b>Band 7</b>		
2807.8	$15^+$	1.05(21)
3646.0	$17^+$	0.45(10)
4603.0	$19^+$	0.26(7)
<b>Band 9</b>		
3456.5	$16^-$	0.68(14)
3828.1	$17^-$	0.42(9)
4251.6	$18^-$	0.23(5)
4716.6	$19^-$	0.22(5)
5219.5	$20^-$	0.15(4)
5752.6	$21^-$	0.11(4)
<b>Band 10</b>		
3139.0	$15^-$	1.3(4)
3181.4	$15^-$	0.9(3)
<b>Band 11</b>		
3046.6	$15^-$	1.15(24)
3953.2	$17^-$	0.75(20)

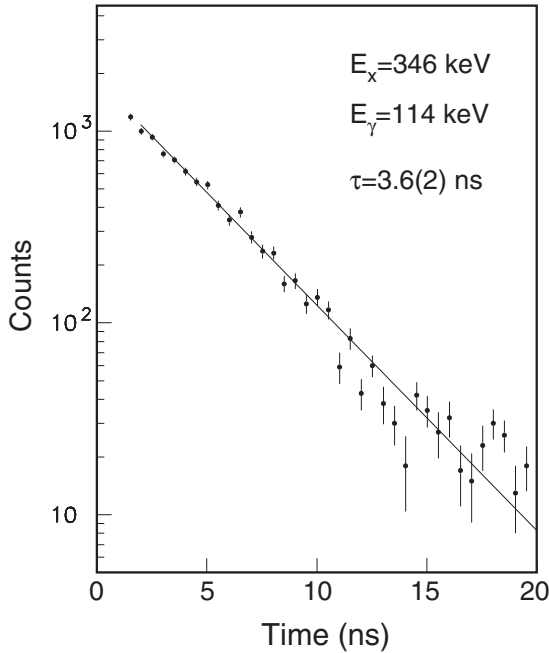


FIG. 8. Time spectrum for the 114-keV transition obtained by the LaBr<sub>3</sub>(Ce) detectors when gating on the 272-keV feeding transition.

identified as an isomeric state with a lifetime of  $\tau(7^+) = 0.38(7)$  ns. The results of this study were reported and discussed in our previous paper [34].

In the present paper we report on the determination of the lifetime for the  $6^-$  state at 345.7-keV excitation energy, band head of band 2 (see Fig. 3). This state is strongly fed by the 271.8-keV transition from the  $7^+$  state, band head of band 1 (see Fig. 1). To derive its lifetime, delayed coincidences between the 271.8-keV  $\gamma$  ray and the deexciting  $\gamma$  ray of 113.7 keV have been investigated. In the spectra created using the LaBr<sub>3</sub>(Ce) detectors the 271.8-keV  $\gamma$  line is not separated from the 279.1-keV  $\gamma$ -ray from the band 1 (see Fig. 4 of Ref. [34]). To clean the spectra, the  $E_{\gamma 1} - E_{\gamma 2} - \Delta T$  cube from the LaBr<sub>3</sub>(Ce) detectors was created with a gate on the 279.1-keV  $\gamma$ -ray in the HPGe detectors. After background subtraction, the slope of time spectrum of the 113.7-keV line has been derived (see Fig. 8). A lifetime of  $\tau = 3.6(2)$  ns has been assigned to the 345.7-keV  $6^-$  band head of band 2.

#### IV. DISCUSSION

In this section we attempt to elucidate the structure of the newly identified bands in <sup>130</sup>La. The experimental properties of the bands, namely the spins of the band heads, the decay patterns, and the transition strengths  $B(M1)$  and  $B(E2)$  are used to assign the configurations.

According to the observed intrinsic configurations in neighboring odd-*A* nuclei, the active single-particle states in <sup>130</sup>La are the  $1/2[550]$ ,  $1/2[420]$ , and  $3/2[422]$  proton states, as well as the  $9/2[514]$ ,  $1/2[411]$ ,  $1/2[400]$ , and  $7/2[404]$  neutron states. Thus, Ref. [46] reports on bands based on the rotation-aligned  $[550]1/2^-$  Nilsson state of  $h_{11/2}$  parentage, as well as bands based on the  $1/2[420]$  and  $3/2[422]$  states

of  $d_{5/2}$  and  $g_{7/2}$  parentage, respectively, in <sup>129</sup>La. Similarly, Ref. [47] reports on a band based on the deformation-aligned  $9/2[514]$  state derived from the  $h_{11/2}$  subshell, a band based on the  $1/2[400]$  and  $1/2[411]$  orbitals from the  $s_{1/2}$  and  $d_{3/2}$  states, and a band based on the  $7/2[404]$  state of  $g_{7/2}$  parentage, in <sup>129</sup>Ba. In the odd-odd <sup>130</sup>La we expect bands that are based on the combinations of the above single-proton and single-neutron states.

In order to understand the structure of the observed states, we have performed calculations using the two-quasiparticles-rotor model (TQRM) code of Ref. [48]. The model Hamiltonian includes the rotational energy of the core and the quasiparticle energies of the odd proton and neutron. The single-particle energies are calculated in a modified oscillator (Nilsson) potential with the  $\kappa$  and  $\mu$  parameters taken from Ref. [49]. The pairing gap and the Fermi levels were derived from a BCS treatment of pairing. The interaction strengths were obtained by multiplying 0.95 to the standard strengths [50] in order to take into account the blocking effect. The core moments of inertia were calculated in such a way that the experimental energy of the  $2^+$  state of the even-even <sup>128</sup>Ba nucleus was reproduced. In evaluation of the electromagnetic moments, an effective  $g_s$  factor of  $0.7g_s^{free}$  has been used and  $g_R$  has been taken as  $Z/A$ . Quadrupole moments of the core were calculated macroscopically. No Coriolis attenuation factor was introduced. Calculations were performed by using various values of quadrupole deformation  $\epsilon_2$  between 0.12 and 0.22. The triaxial parameter was taken  $\gamma = 0^\circ$ , excepting the calculations for the bands 1 and 3, where values between  $0^\circ$  and  $30^\circ$  have been employed.

#### A. Low- and medium-spin states

The low-lying positive-parity states have been calculated with the TQRM assuming that both the valence proton and neutron are located in the deformed *sdg* orbitals of the  $N = 4$  shell. In our previous calculations [43] deformation parameters  $\epsilon_2 = 0.20$  and  $\epsilon_4 = 0.02$  were adopted, as predicted for the <sup>130</sup>La ground state in the macroscopic-microscopic calculations tabulated in Ref. [51]. However, calculations failed to reproduce the spin 3 for the ground state. The present TQRM calculations performed for various  $\epsilon_2$  values indicated that the structure of the low-lying positive-parity states is dominated by the neutron  $7/2[404]$  orbital, coupled with proton deformed orbitals from the  $d_{5/2}$  and  $g_{7/2}$  spherical states. A comparison of the yrast experimental energies with the calculated energies obtained for various quadrupole deformations is illustrated in Fig 9. As seen in this figure, for deformations  $\epsilon_2 \geq 0.15$ , the sequence of the low-lying states is not satisfactorily described. Thus the ground state is calculated to have  $J^\pi = 2^+$ , in contradiction with the experimental  $3^+$  value, while the energy of the  $1^+$  state is predicted higher than the energies of the  $4^+$ ,  $5^+$ , and  $6^+$  states. The description is somewhat improved for lower deformations  $\epsilon_2 \leq 0.14$ , as the  $3^+$  state becomes the ground state, and the  $5^+$  and  $6^+$  states are predicted above the  $1^+$  state. Note that as quoted in Ref. [52], the quadrupole deformation of the Nilsson potential,  $\epsilon_2$ , is related to the quadrupole deformation  $\beta_2$  by the

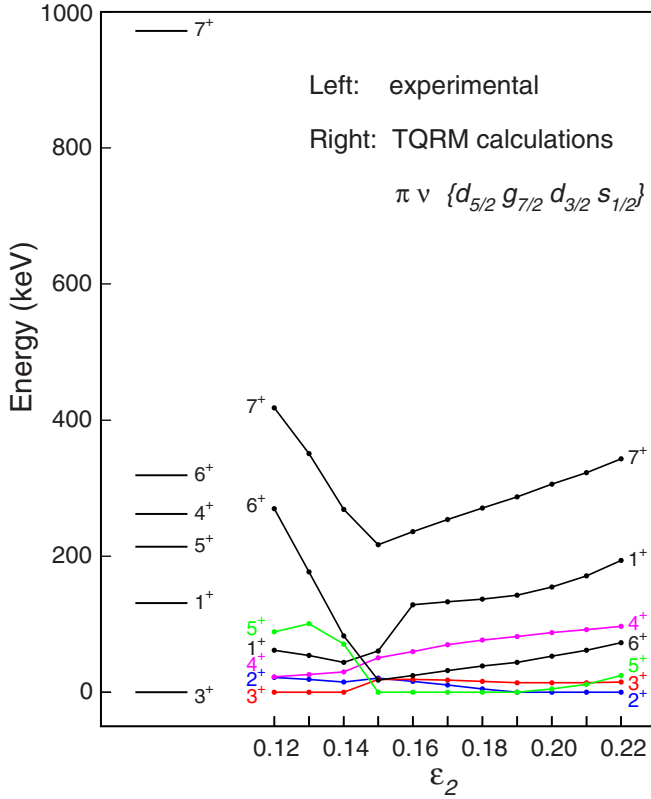


FIG. 9. Experimental low-lying positive-parity states compared to the two-quasiparticles plus rotor model calculations performed for different quadrupole deformations.

relation  $\epsilon_2 = 0.944 \beta_2$ , and thus the value  $\epsilon_2 = 0.14$  corresponds to a deformation  $\beta_2 = 0.15$ .

The negative-parity states in  $^{130}\text{La}$  could arise either by coupling the odd proton in orbitals of the  $h_{11/2}$  subshell with the odd neutron in the  $N = 4$  shell orbitals, or by coupling the odd proton located in the  $sdg$  shell with the odd neutron in the  $h_{11/2}$  subshell. TQRm calculations indicated that medium-spin negative-parity states described by the couplings mentioned above coexist at low-energies. Experimentally an irregular structure of states with spins from  $6^-$  to  $9^-$  was identified (Fig. 1), with 2, 3, or 4 members for each spin value. Based on the assigned configurations for the structures developed on the  $9^-$  states (see below), the states at 988 and 1007 keV are identified as members of the  $\pi h_{11/2} \otimes \nu(sd)$  coupling. The  $9^-$  state at 1122 keV, fed by the 709- and 939-keV cascade  $E2$  transitions deexciting the band 9 is described by the  $\pi g_{7/2} \otimes \nu h_{11/2}$  coupling.

### B. Band deformations

Experimental reduced transition probabilities derived on the basis of the lifetimes measured in this work by applying the DSAM method are given in Table III. The branching ratios have been deduced from the presently determined  $\gamma$ -ray intensities, except for the branchings of the transitions deexciting the level with  $J^\pi = 21^-$  at 5752.6 keV in band 9, that were taken from Ref. [31].

In the case of bands 2 and 9 both  $B(M1)$  and  $B(E2)$  strengths have been deduced. The calculations were done by considering pure  $M1$  transitions. As shown in Sec. III, this is valid for band 9. In the case of band 2 the transitions for which  $B(M1)$  are derived exhibit small  $E2/M1$  mixing, but its influence on the  $B(M1)$  values is less than 5%, much smaller than the assigned errors, and therefore was neglected.

From the  $B(E2)$  values transition quadrupole moments,  $Q_t$ , can be derived using the formula

$$Q_t^2 = \frac{16\pi}{5} \frac{B(E2)}{\langle J_i K 2 0 | J_f K \rangle^2}, \quad (1)$$

where  $J_i$  is the initial spin,  $J_f$  is the final spin, and  $K$  the projection of the total angular momentum on the symmetry axis.

At high spins the transition quadrupole moment is related to the deformation parameters  $\beta_2$  and  $\gamma$  through the relation [53]

$$Q_t = 2\sqrt{\frac{3}{5\pi}} Z e R_0^2 \beta_2 \cos(30^\circ + \gamma), \quad (2)$$

where  $R_0$  is the mean nuclear radius, assumed to have a mass dependence of  $R_0 = 1.2A^{1/3}$ . The derived transition quadrupole moments and  $\beta_2$  values, for  $\gamma = 0^\circ$ , are presented in the last two columns of Table III. The  $K$  values used in the calculation of Clebsch-Gordan coefficients were  $K = 4$  for band 2,  $K = 1$  for bands 7, 10, and 11, and  $K = 6$  for band 9 (see the discussion below).

As seen in Table III for the states with  $J^\pi = 14^- - 17^-$  in band 2 both the  $B(M1)$  and  $B(E2)$  transition strengths have rather similar values. A mean quadrupole deformation  $\beta_2 = 0.165(16)$  has been deduced for these states. At spin  $21^-$  an experimental  $B(M1)$  value much larger has been established, while the  $B(E2)$  value was found somewhat smaller, corresponding to a deformation  $\beta_2 = 0.130(30)$ . A similar quadrupole deformation,  $\beta_2 = 0.133(30)$  was deduced for the  $20^-$  and  $21^-$  states of band 9. For the decoupled bands 10 and 11 a mean deformation value  $\beta_2 = 0.150(15)$  was deduced. On the other hand, larger transition strengths were derived for states of band 7, corresponding to an enhanced deformation,  $\beta_2 = 0.220(17)$ . These results indicate distinct coexisting shapes at high spins in  $^{130}\text{La}$ .

## C. Band configurations

### 1. Positive-parity bands

Bands 1 and 3 are the chiral-candidate doublet bands built on the  $\pi h_{11/2} \otimes \nu h_{11/2}^{-1}$  configuration. We discussed the properties of these bands in Ref. [34] in comparison with the predictions of the two-quasiparticles-plus-rotor model. It was revealed that the calculated  $B(M1)$  values in the yrast band show odd-even spin dependence in the spin range 13–20, in contrast with experimental values, which slightly decrease nearly monotonically with spin. The main conclusion of the study was that the static chirality regime is not realized and that the chirality, if exists, could be of vibrational type. It is worthwhile to mention that the  $B(E2)$  values in the yrast band are somewhat overestimated by the calculations (Fig. 9 of Ref. [34]), indicating that the

TABLE III. Reduced transition probability values, derived using the lifetimes determined in the present work by the Doppler-shift attenuation method and total conversion coefficients taken from Ref. [55]. Branching ratios were obtained from the  $\gamma$ -ray intensities given in Table I, excepting the 5752.6 keV level of band 9, for which the intensities given in Ref. [31] were used. The  $B(M1)$  transition strengths were calculated assuming pure  $M1$  transitions. The last two columns contain the transition quadrupole moments and deformations deduced from experimental reduced transition rates  $B(E2)$ .

$E_i$ (keV)	$J_i^\pi$	$J_f^\pi$	$E_\gamma$ (keV)	$B(M1)$ (W.u.)	$B(E2)$ (W.u.)	$Q_t$ (eb)	$\beta_2$
<b>Band 2</b>							
2200.4	14 <sup>-</sup>	13 <sup>-</sup>	373.1	0.039(12)			
		12 <sup>-</sup>	720.0		44(12)	2.4(3)	0.15(2)
2615.0	15 <sup>-</sup>	14 <sup>-</sup>	414.6	0.054(28)			
		13 <sup>-</sup>	787.6		53(15)	2.6(4)	0.16(3)
3048.5	16 <sup>-</sup>	15 <sup>-</sup>	433.5	0.045(19)			
		14 <sup>-</sup>	848.1		57(18)	2.7(4)	0.17(3)
3519.6	17 <sup>-</sup>	16 <sup>-</sup>	471.1	0.060(30)			
		15 <sup>-</sup>	904.6		56(19)	2.7(5)	0.17(3)
5415.1	21 <sup>-</sup>	20 <sup>-</sup>	464.8	0.348(174)			
		19 <sup>-</sup>	913.0		37(18)	2.1(5)	0.13(3)
<b>Band 7</b>							
2807.8	15 <sup>+</sup>	13 <sup>+</sup>	700.8		118(24)	3.6(4)	0.23(2)
3646.0	17 <sup>+</sup>	15 <sup>+</sup>	838.2		112(25)	3.5(4)	0.22(2)
4603.0	19 <sup>+</sup>	17 <sup>+</sup>	957.0		100(27)	3.3(4)	0.21(3)
<b>Band 9</b>							
3456.5	16 <sup>-</sup>	15 <sup>-</sup>	313.9	1.44(30)			
3828.1	17 <sup>-</sup>	16 <sup>-</sup>	371.6	1.43(31)			
4251.6	18 <sup>-</sup>	17 <sup>-</sup>	423.5	1.78(42)			
4716.5	19 <sup>-</sup>	18 <sup>-</sup>	464.9	1.42(32)			
5219.5	20 <sup>-</sup>	19 <sup>-</sup>	503.0	1.33(53)			
		18 <sup>-</sup>	967.2		31(13)	2.0(5)	0.13(3)
5752.6	21 <sup>-</sup>	20 <sup>-</sup>	533.1	1.46(57)			
		19 <sup>-</sup>	1036.1		37(16)	2.2(5)	0.14(3)
<b>Band 10</b>							
3139.0	15 <sup>-</sup>	13 <sup>-</sup>	790.2		52(16)	2.4(4)	0.15(2)
3181.4	15 <sup>-</sup>	13 <sup>-</sup>	832.6		58(26)	2.5(6)	0.16(4)
<b>Band 11</b>							
3046.6	15 <sup>-</sup>	13 <sup>-</sup>	808.6		53(11)	2.4(3)	0.15(2)
3953.2	17 <sup>-</sup>	15 <sup>-</sup>	906.6		45(12)	2.3(3)	0.14(2)

employed quadrupole deformation,  $\epsilon_2 = 0.2$ , was too large. We performed TQRМ calculations for the  $\pi h_{11/2} \otimes \nu h_{11/2}^{-1}$  configuration using smaller values for the quadrupole deformation parameter. The calculated  $B(M1)$  values were found insensitive to the quadrupole deformation, while the experimental  $B(E2)$  are much better reproduced for a deformation  $\epsilon_2 = 0.14$ .

The doublet states based on the  $\pi h_{11/2} \otimes \nu h_{11/2}^{-1}$  configuration in the odd-odd nuclei around the mass 130 have been described by applying a quadrupole-coupling model [54] that provides an alternative interpretation to the two-quasiparticles-plus-rotor model. In the quadrupole-coupling model the classical core representing the even-even part of the nucleus couples with a neutron and a proton in the  $h_{11/2}$  orbital through a quadrupole-quadrupole interaction. All the necessary properties of the core are provided by the experimental excitation energies, electromagnetic transitions, and moments of the corresponding even-even nuclei. The strengths of the quadrupole-quadrupole interactions are determined from the experimental energy levels of doubly odd

nuclei, and assumed to be smooth functions of the proton number  $Z$  and the neutron number  $N$ . Note that within this model the internal structure of the yrast states was calculated to be quite different from that of the yrare states, in opposition to the chiral interpretation. Good agreement with the experimental data was achieved for both the energy spectra and features of electromagnetic transitions in odd-odd Cs, La, and Pr nuclei. In particular the calculated  $B(M1)$  strengths in the yrast band of  $^{130}\text{La}$  show a smooth spin dependence, in accordance with our experimental results [34].

The newly identified structure labeled as band 4 feeds the  $12^+$  state of band 3. The  $B(M1; J \rightarrow J-1)/B(E2; J \rightarrow J-2)$  value,  $2.0(7) \mu_N^2/e^2b^2$ , was determined in this band for spin  $J = 15$  by using transition energies and intensities. This ratio is similar with the values derived at the same spin in the bands 1 and 3, namely  $2.9(9)$  and  $2.6(10) \mu_N^2/e^2b^2$ , respectively, indicating that the configuration of band 4 is  $\pi h_{11/2} \otimes \nu h_{11/2}^{-1}$ , similar to the configurations of bands 1 and 3. The energy separation between the bands 3 and 4,  $\Delta E(J) = E_{b4}(J) - E_{b3}(J)$ , is rather constant, about 150 keV. This is

considerably smaller than the  $\Delta E$  values for bands 3 and 1, that amount to approximately 350 keV (see Fig. 6(a) of Ref. [34]). The mean separation energy of the doublets depends on the degree of the chiral symmetry breaking [56], and therefore one could expect that band 3 and the newly established band 4, with small energy separation, are chiral partner bands. It is worthwhile to mention that triplet bands with the same configuration were identified in several nuclei with chiral-candidate bands. In the odd-odd  $^{134}\text{Pr}$  nucleus a third  $\pi h_{11/2} \otimes \nu h_{11/2}^{-1}$  band was observed up to spin  $J = 19$  [24], and it was suggested that this band is the chiral partner of the previously known side band. Triplet bands with the same configuration,  $\pi g_{9/2} \nu h_{11/2} (g_{7/2} d_{5/2})$ , were reported in odd-mass  $^{105}\text{Rh}$  [57] and  $^{105}\text{Ag}$  [58], with the second and third bands interpreted as chiral doublet bands [59]. In order to test whether band 4 in  $^{130}\text{La}$  stands as a chiral-partner, it would be important to extend it at higher spins in a new high-statistics experiment.

Band 5 is a  $\Delta J = 1$  band whose members decay by in-band  $M1$  and  $E2$  transitions, as well as by dipole transitions to states of band 1. The  $B(M1; J \rightarrow J-1)/B(E2; J \rightarrow J-2)$  ratio has values of 3.2(13)  $\mu_N^2/e^2b^2$  and 5.7(31)  $\mu_N^2/e^2b^2$  at spin 12 and 13, respectively, similar to those of band 1. This similarity, as well as the connection with band 1, suggest that band 5 is described by the  $\pi h_{11/2} \otimes \nu h_{11/2}^{-1}$  configuration. The dipole band 6 linked to band 5 could also involve the same configuration.

The new band 7 is a decoupled band characterized by a quadrupole deformation  $\beta_2 = 0.220(17)$  significantly larger than the values  $\beta_2 = 0.13\text{--}0.16$  derived for the other bands in  $^{130}\text{La}$  (see Table III). In this mass region it was shown that structures that involve the  $(f_{7/2}h_{9/2})\Omega = 1/2$  neutron orbital have an enhanced deformation compared to the normally deformed bands. We performed TQRM calculations, by coupling the proton in the  $h_{11/2}$  orbital with the neutron in the  $(f_{7/2} + h_{9/2})$  orbitals. The used deformation parameters were  $\epsilon_2 = 0.21$  and  $\gamma = 0^\circ$ . The calculations revealed that the  $f_{7/2}$  and  $h_{9/2}$  neutron orbitals, corresponding to the 1/2[530] and 1/2[541] Nilsson states, are strongly mixed. The coupling of these neutron states with the 1/2[550] proton state produces two independent decoupled bands, with the even-spin band lower in energy. By including the proton 3/2[541] state the two decoupled bands, with odd-spin and with even spin, appear at almost identical energies. The observed bands 7 and 8 in  $^{130}\text{La}$  could be therefore described by coupling the proton in the low- $\Omega$  states of the  $h_{11/2}$  orbital with the neutron in the  $(f_{7/2}h_{9/2})\Omega = 1/2$  states. Up to now only few nuclei in the region were found to exhibit decoupled bands involving these neutron states, namely the odd-odd  $^{130,132,134}\text{Pr}$  ( $Z = 59$ ,  $N = 71, 73, 75$ ) [23,26] and  $^{134}\text{Pm}$  ( $Z = 61$ ,  $N = 73$ ) [25], and the odd-mass  $^{133}\text{Nd}$  ( $Z = 60$ ,  $N = 73$ ) [22]. From lifetime measurements it was shown that these decoupled bands show an increased deformation, for example in  $^{130}\text{Pr}$  and  $^{132}\text{Pr}$  they have quadrupole deformations  $\beta_2 = 0.24\text{--}0.26$ , which are larger than  $\beta_2 = 0.19\text{--}0.20$  measured for the normally deformed bands in these nuclei [23]. The deformations derived in the present work for  $^{130}\text{La}$  are somewhat smaller both for normal and intruder bands. They provide new information on the shape-driving behavior of the 1/2[530]

and 1/2[541] intruder neutron states in the  $A \approx 130$  mass region.

## 2. Negative-parity two-quasiparticle bands

Band 2, the yrast negative-parity band, was described by coupling the proton rotation-aligned 1/2[550] Nilsson state of  $h_{11/2}$  parentage with the neutron 7/2[404] state of  $g_{7/2}$  parentage [30]. A value of  $K = 4$  was used in Eq. (1) for calculating the transition quadrupole moments of Table III.

For the newly identified bands 10 and 11 a doubly decoupled nature is suggested, as only the odd-spin states of the bands were observed. They could arise by coupling the proton 1/2[550] Nilsson state with neutron low- $\Omega$  orbitals from the  $d_{3/2}s_{1/2}$  states. The transition quadrupole moments in Table III were estimated using  $K = 1$ .

TQRM calculations, performed with the odd proton in the  $h_{11/2}$  subshell and the odd neutron in the  $N = 4$  shell orbitals, predicted the occurrence of almost independent structures that could be associated with the experimental ones. All calculated bands involve the proton occupying the 1/2[550] and 3/2[541] orbitals. The structure of the lowest-lying band, assigned to band 2, is dominated by the neutron in the 7/2[404] orbital, with contributions from the 5/2[402] and 5/2[413] orbitals from the  $d_{5/2}$  and  $g_{7/2}$  parentage, respectively. A comparison between the experimental levels and reduced transition probabilities of band 2 and those predicted by TQRM calculations is shown in Fig. 10. Both  $B(M1)$  and  $B(E2)$  reduced transition probabilities are well reproduced by the calculations, excepting the  $21^-$  level, for which the experimental  $B(M1)$  is much larger than the calculated one, while the experimental  $B(E2)$  is smaller.

It is worth noting that in the previous study of Ref. [30] a backbend was found for this band at  $\hbar\omega = 0.46$  MeV, that was attributed to aligning  $h_{11/2}$  neutrons. It was suggested that an increase in the  $B(M1)$  value would be expected through an increase of the nuclear magnetic dipole moment. Total Routhian surface calculations [30] predict a change from the axial symmetric shape to negative  $\gamma$  and also a decrease in the deformation  $\beta_2$  of 10–20%, which would affect the  $B(E2)$  value. Our results derived for the  $21^-$  level, where the backbend occurs, nicely confirm the above predictions.

The second and third bands predicted by the TQRM calculations involve the odd neutron occupying mainly the low- $\Omega$  orbitals (1/2, 3/2) from the  $d_{3/2}s_{1/2}$  states, and they can be associated with the bands 10 and 11. A comparison between the experimental and calculated results for band 11 is illustrated in Fig. 11. The experimental reduced transition probabilities  $B(E2)$  are well reproduced by the calculated values. The calculations predict a large signature splitting with the even-spin unfavored component much higher in energy. The predicted  $B(M1)$  strengths for transitions from odd-spin states to even-spin states are extremely small, and therefore the  $\gamma$ -ray intensities in the unfavored branch is expected to be much smaller than that in the favored branch. It is worth noting that a negative-parity decoupled band has been reported also in the neighbor  $^{132}\text{La}$ , described by the same configuration as in the present case [60,61]. In a subsequent higher statistics experiment devoted to the high-spin states in

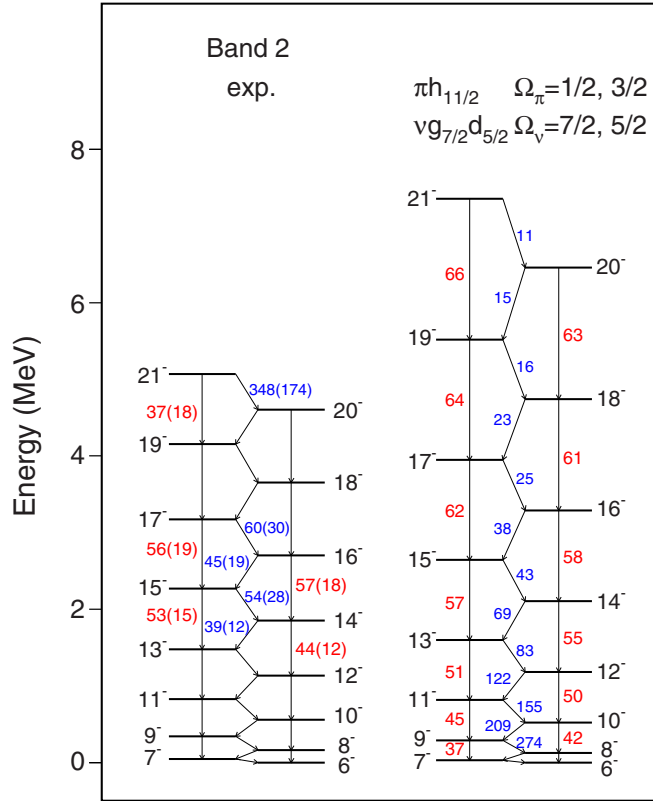


FIG. 10. Experimental band 2 compared to the two-quasiparticles plus rotor model calculations for quadrupole deformation  $\epsilon_2 = 0.14$ . The  $B(E2)$  values, expressed in W.u., are shown in red color, while the  $B(M1)$  values, expressed in mW.u., are shown in blue color.

$^{132}\text{La}$  [62] the odd-spin decoupled band was confirmed, and moreover the much weaker even-spin unfavored branch was identified (band 5 of Ref. [62]). Only  $M1$  transitions from the even-spin states to odd spin-states could be observed, in accordance with TQRM predictions.

The 345.7-keV  $6^-$  isomeric state, band head of band 2, is deexcited by the transitions of 113.7 and 109.1 keV towards lower-lying  $6^-$  states, and by the transition of 26.6 keV towards the  $6^+$  state. By using the intensities given in Ref. [44] and the present work, and the total conversion coefficients taken from Ref. [55], the reduced transition probabilities for these transitions were determined as:

$$\begin{aligned} B(E1)(26.6 \text{ keV}) &= 9.6(12) \times 10^{-4} \text{ W.u.}, \\ B(M1)(113.7 \text{ keV}) &= 1.8(3) \times 10^{-3} \text{ W.u.}, \\ B(M1)(109.1 \text{ keV}) &= 1.3(5) \times 10^{-4} \text{ W.u.} \end{aligned}$$

The hindrances of the  $M1$  transitions could be understood based on the configurations of the  $6^-$  states. Transition strengths of about 0.1 mW.u. were estimated within TQRM for the transitions from the  $6^-$  band head of band 2 to the  $6^-$  neighboring predicted states, in good agreement with the experimental values.

### 3. Negative-parity four-quasiparticle band

Band 9 is a dipole band involving large  $B(M1)$  strengths, roughly constant with increasing spin. In view of the high

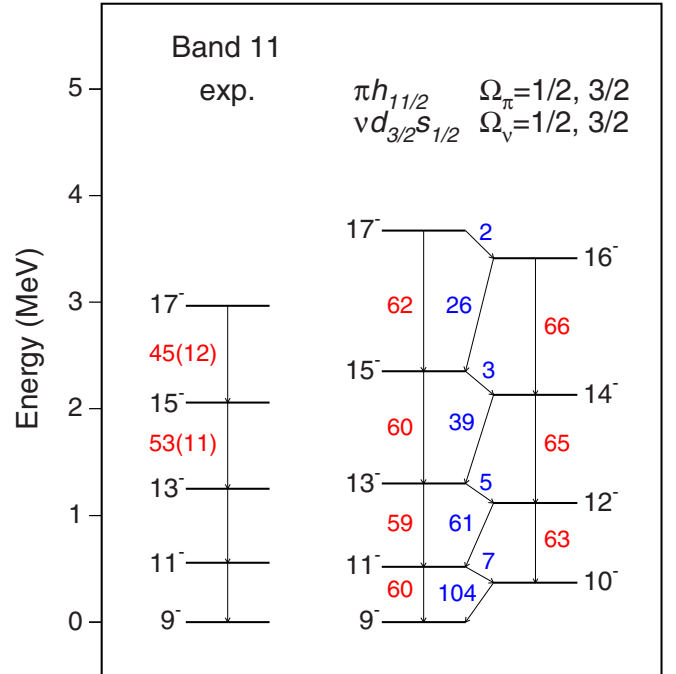


FIG. 11. Experimental decoupled band 11 compared to the two-quasiparticles plus rotor model calculations for quadrupole deformation  $\epsilon_2 = 0.14$ . The experimental and calculated  $B(E2)$  values, expressed in W.u., are shown in red color, while the calculated  $B(M1)$  values, expressed in mW.u., are shown in blue color.

value of bandhead spin  $13^-$  and energy 2770 keV, it should be a multiparticle band. Three possible four-quasiparticle configurations were considered,  $\pi h_{11/2} \otimes \nu g_{7/2}(h_{11/2})^2$ ,  $\pi g_{7/2} \otimes \nu h_{11/2}(h_{11/2})^2$ , and  $\pi g_{7/2}(h_{11/2})^2 \otimes \nu h_{11/2}$ . The experimental  $B(M1)$  values were interpreted by the semiclassical calculations based on the geometrical model of Dönau and Frauendorf [63].

The  $B(M1)$  values for  $\Delta J = 1$  transitions are given by the expression [63,64]

$$B(M1) = (3/8\pi)\mu_{\perp}^2, \quad (3)$$

where  $\mu_{\perp}^2$  is the component of the magnetic moment  $\vec{\mu}$  perpendicular to the total angular momentum  $\vec{J}$ .

In our case the total magnetic moment is given by the components of the odd proton  $\pi$ , odd neutron  $\nu$ , the two aligned particles  $2p$ , and the core  $R$ . The component of the magnetic moment perpendicular on  $\vec{J}$  is

$$\mu_{\perp} = (g_j^{(\pi)} - g_R)j_{\perp}^{\pi} + (g_j^{(\nu)} - g_R)j_{\perp}^{\nu} + (g_j^{(2p)} - g_R)j_{\perp}^{2p}. \quad (4)$$

Using the explicit expressions given in Ref. [65] for the perpendicular components of angular momenta  $j_{\perp}$  we calculated  $B(M1)$  values for the configurations mentioned above. We adopted the values of  $K_i$  (projection on the symmetry axis) and  $i_i$  (projection on rotation axis) given in Ref. [62] for  $^{132}\text{La}$ . The used values were  $K_{\pi} = 1.5$ ,  $i_{\pi} = 4.5$  for  $\pi h_{11/2}$ ;  $K_{\pi} = 2.5$ ,  $i_{\pi} = 1.5$  for  $\pi g_{7/2}$ ;  $K_{\nu} = 4.5$ ,  $i_{\nu} = 2$  for  $\nu h_{11/2}$ ;  $K_{\nu} = 3.5$ ,  $i_{\nu} = 1$  for  $\nu g_{7/2}$ . The two protons (neutrons) were considered to be fully aligned,  $i_{2p} = 9$ . The gyromagnetic

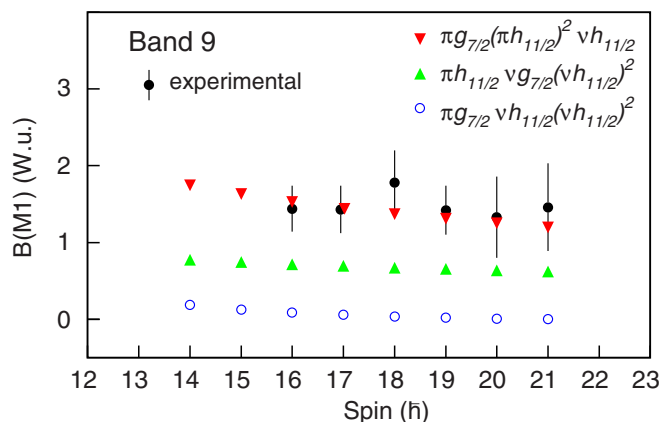


FIG. 12. Experimental  $B(M1)$  values derived for states of band 9 compared to calculated values for the candidate configurations.

ratios  $g_j$  were calculated with an effective  $g_s$  factor of  $0.7g_s^{free}$  and  $g_R$  has been taken as  $Z/A$ .

The experimental  $B(M1)$  values in band 9 are compared with the estimated values in Fig. 12. We note the excellent agreement between the experimental values and those calculated for the  $\pi g_{7/2}(h_{11/2})^2 \otimes \nu h_{11/2}$  configuration involving two aligned protons. For the other two configurations, that involve two aligned neutrons, the calculated values are much smaller.

It is interesting to note that a negative-parity dipole band was reported in odd-odd  $^{132}\text{La}$  [62], with crossover  $E2$  transitions observed for spins  $\geq 16^-$ . Differently from our case, the bands feed states of the positive-parity  $\pi h_{11/2} \otimes \nu h_{11/2}$  band. No lifetimes were reported for that band, however, on the basis of  $B(M1)/B(E2)$  ratios the same  $\pi g_{7/2}(h_{11/2})^2 \otimes \nu h_{11/2}$  configuration was proposed.

As seen in Table III the quadrupole moment of the  $20^-$  and  $21^-$  states,  $Q_t = 2.1(5)$  eb, and the corresponding quadrupole deformation  $\beta_2 = 0.13(3)$  in band 9 are similar with the value derived for the  $21^-$  state in band 2. This stands as a nice experimental confirmation of the shape change associated with the alignment of two high- $\Omega$  orbitals.

## V. SUMMARY

The medium- and high-spin structure of  $^{130}\text{La}$  was studied using the  $^{121}\text{Sb}(^{12}\text{C}, 3n)$  reaction with the ROSPHERE array at IFIN-HH, Bucharest. The existing level scheme of  $^{130}\text{La}$

was confirmed and significantly extended with the addition of seven new bands. By applying the Doppler-shift attenuation method the lifetimes of 18 high-spin states in five bands have been determined. A lifetime of  $\tau = 3.6$  ns has been measured for the 346-keV  $6^-$  state by the in-beam fast timing technique. The experimental properties of both low- and high-spin states were compared with theoretical calculations done in the frame of the two-quasiparticles-plus-rotor model. The observed sequence of positive-parity low-lying states was reproduced for a quadrupole deformation of the Nilsson potential  $\epsilon_2 = 0.14$ . This deformation, compatible with that derived from  $B(E2)$  measurements, is smaller than the deformation  $\epsilon_2 = 0.20$  given by the macroscopic-microscopic calculations of Ref. [51]. State-of-the-art calculations with a self-consistent total Routhian surface model would be necessary to understand if the observed deformation is predicted by the mean-field models. Negative-parity decoupled bands 10 and 11 having a quadrupole deformation  $\beta_2 = 0.150(15)$  were interpreted by coupling the proton in the  $1/2[550]$  and  $3/2[541]$  orbitals with the odd neutron occupying mainly the low- $\Omega$  orbitals ( $1/2, 3/2$ ) from the  $d_{3/2}s_{1/2}$  states. The positive-parity decoupled band 7 exhibits a larger deformation,  $\beta_2 = 0.220(17)$ , and was described as involving the intruder  $\pi h_{11/2} \otimes \nu(f_{7/2} + h_{9/2})$  configuration. This provides the first evidence on the presence of the shape-driving  $(f_{7/2} + h_{9/2})\Omega = 1/2$  intruder neutron orbitals in a lanthanum isotope. The high-spin dipole band 9, connected with the lower-lying known states, exhibits large experimental  $B(M1)$  values, around 1.5 W.u.. They were remarkably well reproduced by values calculated applying the geometrical model of Dönau and Frauendorf for the multiparticle configuration  $\pi g_{7/2}(h_{11/2})^2 \otimes \nu(h_{11/2})$  involving two aligned protons. The high-spin positive-parity band 4, linked with the band 3, was assigned the same  $\pi h_{11/2} \otimes \nu h_{11/2}^{-1}$  configuration. To test whether this band is a chiral partner, it would be of interest to extend it at higher spins in a new high-statistics experiment.

## ACKNOWLEDGMENTS

Authors are thankful to the FN Tandem staff of the Horia Hulubei National Institute of Physics and Nuclear Engineering for the good quality delivered beam. This work was supported by the Ministry of Education and Research, Romania, Contract No. PN-19-06-01-02.

[1] S. Frauendorf and J. Meng, *Nucl. Phys. A* **617**, 131 (1997).  
 [2] B. W. Xiong and Y. Y. Wang, *At. Data Nucl. Data Tables* **125**, 193 (2019).  
 [3] A. D. Ayangeakaa, U. Garg, M. D. Anthony, S. Frauendorf, J. T. Matta, B. K. Nayak *et al.*, *Phys. Rev. Lett.* **110**, 172504 (2013).  
 [4] C. M. Petrache, Q. B. Chen, S. Guo, A. D. Ayangeakaa, U. Garg, J. T. Matta *et al.*, *Phys. Rev. C* **94**, 064309 (2016).  
 [5] S. Zhu *et al.*, *Phys. Rev. Lett.* **91**, 132501 (2003).  
 [6] B. F. Lv, C. M. Petrache, Q. B. Chen, J. Meng, A. Astier, E. Dupont *et al.*, *Phys. Rev. C* **100**, 024314 (2019).

[7] C. M. Petrache, B. F. Lv, A. Astier, E. Dupont, Y. K. Wang, S. Q. Zhang *et al.*, *Phys. Rev. C* **97**, 041304(R) (2018).  
 [8] C. M. Petrache *et al.*, *Phys. Rev. C* **86**, 044321 (2012).  
 [9] J. Peng, J. Meng, and S. Q. Zhang, *Phys. Rev. C* **68**, 044324 (2003).  
 [10] T. Koike, K. Starosta, and I. Hamamoto, *Phys. Rev. Lett.* **93**, 172502 (2004).  
 [11] K. Starosta, C. J. Chiara, D. B. Fossan, T. Koike, T. T. S. Kuo, D. R. LaFosse, S. G. Rohoziński, Ch. Droste, T. Morek, and J. Srebrny, *Phys. Rev. C* **65**, 044328 (2002).

- [12] T. Marchlewski *et al.*, *Acta Phys. Pol. B* **46**, 689 (2015).
- [13] K. Selvakumar, A. K. Singh, C. Ghosh, P. Singh, A. Goswami, R. Raut *et al.*, *Phys. Rev. C* **92**, 064307 (2015).
- [14] E. Grodner, J. Srebrny, A. A. Pasternak, I. Zalewska, T. Morek, Ch. Droste *et al.*, *Phys. Rev. Lett.* **97**, 172501 (2006).
- [15] E. Grodner *et al.*, *Phys. Lett. B* **703**, 46 (2011).
- [16] W. Xiaoguang *et al.*, *Plasma Sci. Technol.* **14**, 526 (2012).
- [17] D. Tonev, G. de Angelis, P. Petkov, A. Dewald, S. Brant, S. Frauendorf *et al.*, *Phys. Rev. Lett.* **96**, 052501 (2006).
- [18] B. Singh, R. Zywna, and R. B. Firestone, *Nucl. Data Sheets* **97**, 241 (2002).
- [19] R. Wyss, J. Nyberg, A. Johnson, R. Bengtsson, and W. Nazarewicz, *Phys. Lett. B* **215**, 211 (1988).
- [20] E. S. Paul, P. T. W. Choy, C. Andreoiu, A. J. Boston, A. O. Evans, C. Fox *et al.*, *Phys. Rev. C* **71**, 054309 (2005).
- [21] K. Hauschild *et al.*, *Phys. Rev. C* **50**, 707 (1994).
- [22] D. Bazzacco *et al.*, *Phys. Rev. C* **58**, 2002 (1998).
- [23] F. G. Kondev, M. A. Riley, D. J. Hartley, T. B. Brown, R. W. Laird, M. Lively *et al.*, *Phys. Rev. C* **59**, 3076 (1999).
- [24] J. Timár, K. Starosta, I. Kuti, D. Sohler, D. B. Fossan, T. Koike *et al.*, *Phys. Rev. C* **84**, 044302 (2011).
- [25] R. Wadsworth, S. M. Mullins, P. J. Bishop, A. Kirwan, M. J. Godfrey, P. J. Nolan, and P. H. Regan, *Nucl. Phys. A* **526**, 188 (1991).
- [26] M. N. Rao, R. V. Ribas, N. H. Medina, J. R. B. Oliveira, M. A. Rizzutto, W. A. Seale *et al.*, *Phys. Rev. C* **58**, R1367 (1998).
- [27] F. Brandolini *et al.*, *Phys. Rev. C* **60**, 024310 (1999).
- [28] R. W. Laird, F. G. Kondev, M. A. Riley, D. E. Archer, T. B. Brown, R. M. Clark *et al.*, *Phys. Rev. Lett.* **88**, 152501 (2002).
- [29] E. S. Paul, C. W. Beausang, D. B. Fossan, R. Ma, W. F. Piel, Jr., N. Xu, and L. Hildingsson, *Phys. Rev. C* **36**, 1853 (1987).
- [30] M. J. Godfrey, Y. He, I. Jenkins, A. Kirwan, P. J. Nolan, D. J. Thornley, S. M. Mullins, and R. Wadsworth, *J. Phys. G: Nucl. Part. Phys.* **15**, 487 (1989).
- [31] M. J. Godfrey, Y. He, I. Jenkins, A. Kirwan, P. J. Nolan, D. J. Thornley, S. M. Mullins, R. Wadsworth, and R. A. Wyss, *J. Phys. G: Nucl. Part. Phys.* **15**, 671 (1989).
- [32] M. J. Godfrey, Y. He, I. Jenkins, A. Kirwan, P. J. Nolan, R. Wadsworth, and S. M. Mullins, *J. Phys. G: Nucl. Part. Phys.* **15**, L163 (1989).
- [33] T. Koike, K. Starosta, C. J. Chiara, D. B. Fossan, and D. R. LaFosse, *Phys. Rev. C* **63**, 061304(R) (2001).
- [34] M. Ionescu-Bujor, S. Aydin, N. Mărginean, C. Costache, D. Bucurescu, N. Florea *et al.*, *Phys. Rev. C* **98**, 054305 (2018).
- [35] D. Bucurescu *et al.*, *Nucl. Instrum. Methods Phys. Res. Sect. A* **837**, 1 (2016).
- [36] M. Piiparinen *et al.*, *Nucl. Phys. A* **605**, 191 (1996).
- [37] J. C. Wells and N. R. Johnson, Report No. ORNL-6689, 1991, p. 44.
- [38] J. F. Ziegler, *The Stopping and Range of Ions in Matter*, Vols. 3 and 5 (Pergamon Press, Oxford, 1980).
- [39] J. F. Ziegler, J. P. Biersack, and V. Littmark, *The Stopping Power and Range of Ions in Solid*, Vol. 1 (Pergamon Press, Oxford, 1985).
- [40] E. Grodner *et al.*, *Eur. Phys. J. A* **27**, 325 (2006).
- [41] I. Sankowska *et al.*, *Eur. Phys. J. A* **37**, 169 (2008).
- [42] N. Mărginean *et al.*, *Eur. Phys. J. A* **46**, 329 (2010).
- [43] M. Ionescu-Bujor, A. Iordăchescu, N. Mărginean, R. Lica, D. Bucurescu, F. Brandolini *et al.*, *Phys. Rev. C* **90**, 014323 (2014).
- [44] M. Ionescu-Bujor, A. Iordăchescu, N. Mărginean, R. Lica, D. Bucurescu, F. Brandolini *et al.*, *Phys. Rev. C* **90**, 029903(E) (2014).
- [45] P. M. Endt, *At. Data Nucl. Data Tables* **26**, 47 (1981).
- [46] Y. He, M. J. Godfrey, I. Jenkins, A. J. Kirwan, S. M. Mullins, P. J. Nollan, E. S. Paul, and R. Wadsworth, *J. Phys. G: Nucl. Part. Phys.* **18**, 99 (1992).
- [47] A. P. Byrne, K. Schiffer, G. D. Dracoulis, B. Fabricius, T. Kibédi, A. E. Stuchbery, and K. P. Lieb, *Nucl. Phys. A* **548**, 131 (1992).
- [48] P. B. Semmes and I. Ragnarsson, *Conference on High Spin Physics and  $\gamma$ -Soft Nuclei*, Pittsburg, 1990 (World Scientific, Singapore, 1991), p. 500.
- [49] J.-Y. Zhang, N. Xu, D. B. Fossan, Y. Liang, R. Ma, and E. S. Paul, *Phys. Rev. C* **39**, 714 (1989).
- [50] S. G. Nilsson, C. F. Tsang, A. Sobczewski, Z. Szymański, S. Wycech, C. Gustafsson, I.-L. Lamm, P. Möller and B. Nilsson, *Nucl. Phys. A* **131**, 1 (1969).
- [51] P. Möller, J. R. Nix, W. D. Myers, and W. J. Swiatecki, *At. Data Nucl. Data Tables* **59**, 185 (1995).
- [52] R. Bengtsson, J. Dudek, W. Nazarewicz, and P. Olanders, *Phys. Scr.* **39**, 196 (1989).
- [53] H. Emling, E. Grosse, R. Kulesa, D. Schwalm, and H. J. Wollersheim, *Nucl. Phys. A* **419**, 187 (1984).
- [54] K. Higashiyama and N. Yoshinaga, *Eur. Phys. J. A* **33**, 355 (2007).
- [55] T. Kibédi, T. W. Burrows, M. B. Trzhaskovskaya, P. M. Davidson, and C. W. Nestor Jr., *Nucl. Instrum. Meth. Phys. Res. A* **589**, 202 (2008).
- [56] E. Grodner, S. G. Rohoziński, and J. Srebrny, *Acta Phys. Pol. B* **38**, 1411 (2007).
- [57] J. A. Alcántara-Núñez *et al.*, *Phys. Rev. C* **69**, 024317 (2004).
- [58] J. Timár *et al.*, *Phys. Rev. C* **76**, 024307 (2007).
- [59] H. Jia, B. Qi, C. Liu, and S.-Yu. Wang, *J. Phys. G: Nucl. Part. Phys.* **46**, 035102 (2019).
- [60] V. Kumar, P. Das, R. P. Singh, S. Muralithar, and R. K. Bhowmik, *Eur. Phys. J. A* **17**, 153 (2003).
- [61] V. Kumar, P. Das, S. Lakshmi, P. K. Joshi, H. C. Jain, R. P. Singh, R. Kumar, S. Muralithar, and R. K. Bhowmik, *Phys. Rev. C* **82**, 054302 (2010).
- [62] I. Kuti, J. Timár, D. Sohler, E. S. Paul, K. Starosta, A. Astier *et al.*, *Phys. Rev. C* **87**, 044323 (2013).
- [63] F. Dönaу and S. Frauendorf, in *Proceedings of the International Conference on High Angular Momentum Properties of Nuclei, Oak Ridge, 1982*, edited by N. R. Johnson (Harwood, New York, 1983), p. 143.
- [64] F. Dönaу, *Nucl. Phys. A* **471**, 469 (1987).
- [65] V. Kumar, Pragya Das, R. P. Singh, R. Kumar, S. Muralithar, and R. K. Bhowmik, *Phys. Rev. C* **76**, 014309 (2007).